

Distribution Agreement

In presenting this thesis or dissertation as a partial fulfillment of the requirements for an advanced degree from Emory University, I hereby grant to Emory University and its agents the non-exclusive license to archive, make accessible, and display my thesis or dissertation in whole or in part in all forms of media, now or hereafter known, including display on the world wide web. I understand that I may select some access restrictions as part of the online submission of this thesis or dissertation. I retain all ownership rights to the copyright of the thesis or dissertation. I also retain the right to use in future works (such as articles or books) all or part of this thesis or dissertation.

Signature:

Ian Tamargo

Date

**The Role of Shear-Sensitive Protein Heart of Glass Homolog 1 (HEG1) in Endothelial
Biology and Atherosclerosis**

By

Ian Tamargo
Doctor of Philosophy

Graduate Division of Biological and Biomedical Science
Molecular and Systems Pharmacology

Hanjoong Jo, Ph.D.
Advisor

Kathy Griendling, Ph.D.
Committee Member

Khalid Salaita, Ph.D.
Committee Member

Roy Sutliff, Ph.D.
Committee Member

W. Robert Taylor, M.D., Ph.D.
Committee Member

Accepted:

Kimberly Jacob Arriola, Ph.D., M.P.H.
Dean of the James T. Laney School of Graduate Studies

Date

**The Role of Shear-Sensitive Protein Heart of Glass Homolog 1 (HEG1) in Endothelial
Biology and Atherosclerosis**

By

Ian Tamargo
A.B., Princeton University, 2014

Advisor: Hanjoong Jo, Ph.D.

An abstract of
A dissertation submitted to the Faculty of the
James T. Laney School of Graduate Studies of Emory University
in partial fulfillment of the requirements for the degree of
Doctor of Philosophy
in Graduate Division of Biological and Biomedical Science
Molecular and Systems Pharmacology
2023

Abstract

The Role of Shear-Sensitive Protein Heart of Glass Homolog 1 (HEG1) in Endothelial Biology and Atherosclerosis

By Ian Tamargo

Atherosclerotic diseases such as myocardial infarction, ischemic stroke, and peripheral arterial disease continue to be leading causes of death worldwide despite the success of cholesterol-lowering drugs and drug-eluting stents, raising the dire need to identify additional therapeutic targets. Interestingly, atherosclerosis preferentially develops in curved and branching arterial regions, where endothelial cells are exposed to disturbed blood flow with characteristic low-magnitude and oscillatory shear stress. In contrast, straight arterial regions exposed to stable flow, associated with high-magnitude, unidirectional shear stress, are relatively well protected from the disease through shear-dependent, atheroprotective endothelial responses, such as induction of atheroprotective protein expression. In the current study, heart of glass homolog 1 (HEG1) is identified as a stable flow-induced endothelial protein. HEG1 is an endothelial-enriched single-pass transmembrane glycoprotein that is essential for vascular development and integrity. Due to its demonstrated importance in vascular biology, and its induction by stable flow, HEG1 was hypothesized to mediate atheroprotective endothelial responses to stable flow and protect against atherosclerotic plaque formation. To test this hypothesis, mechanistic and functional responses to stable flow in endothelial cells with and without HEG1 expression were compared using an *in vitro* cone and plate shear system. HEG1 expression was found to be necessary for stable flow-induced Krüppel-like factor 2 and 4 (KLF2/4) expression, two critical transcription factors that control the majority of flow-sensitive endothelial genes. HEG1 expression was also required to mediate the pro-alignment, anti-inflammatory, anti-permeability, anti-migratory and anti-angiogenic effects of stable flow. Using the *in vivo* partial carotid ligation model of acute atherosclerosis, inducible endothelial cell HEG1 knockout mice (HEG1^{iECKO}) were found to have decreased endothelial KLF2/4 expression, and to have more extensive atherosclerotic plaques as compared to controls. Together, these data indicate that HEG1 protein is required to mediate many atheroprotective effects of stable flow via control of KLF2/4 expression, and that HEG1 is a promising new therapeutic target for atherosclerosis.

**The Role of Shear-Sensitive Protein Heart of Glass Homolog 1 (HEG1) in Endothelial
Biology and Atherosclerosis**

By

Ian Tamargo
A.B., Princeton University, 2014

Advisor: Hanjoong Jo, Ph.D.

A dissertation submitted to the Faculty of the
James T. Laney School of Graduate Studies of Emory University
in partial fulfillment of the requirements for the degree of
Doctor of Philosophy
in Graduate Division of Biological and Biomedical Science
Molecular and Systems Pharmacology
2023

Acknowledgements

I would first and foremost like to thank Dr. Jo for welcoming me into his laboratory and mentoring me week in, week out for the past five years. I have learned a tremendous amount from him about science, communication, professionalism and life, and will always keep these lessons with me. I would also like to thank Dong Won Kang, Sunkum Kang, Sandeep Kumar, Colleen Spellen and all of the amazing lab mates and friends I have had the pleasure of working with over the past five years. I would especially like to thank Chenbo Xu, Kyung In Baek, Juyoung Kim, Yerin Kim, Rachel Choi and Janie Johnson for their work on the HEG1 project. Furthermore, I thank the members of my thesis committee, Dr. Griendling, Dr. Salaita, Dr. Taylor and Dr. Sutliff for their help in guiding my thesis project, as well as the faculty and staff of the Molecular and Systems Pharmacology program for their teaching and guidance.

Personally, I would like to thank my wife, Angela, as well as my parents, Rafael and Terry, and brother, Rafi for always supporting me throughout all of the ups and downs of my graduate school career!

Thank you all!

Table of Contents

<i>Acknowledgements</i>	<i>VI</i>
<i>Table of Contents</i>	<i>VII</i>
<i>List of Figures</i>	<i>IX</i>
<i>List of Tables</i>	<i>X</i>
<i>List of Abbreviations</i>	<i>XI</i>
1 Introduction	1
1.1 Background	1
1.1.1 Atherosclerosis	1
1.1.2 Disturbed blood flow induces atherosclerosis	3
1.1.3 Flow potently regulates EC function	7
1.1.4 Mechanosensors and mechanosignal transduction in endothelial cells	9
1.1.5 OMICs approaches to determine flow-sensitive endothelial genes, proteins, and pathways	15
1.1.6 Therapeutic implications of flow-sensitive genes, proteins, and pathways in atherosclerosis	17
1.2 Hypothesis and Specific Aims	20
1.2.1 Hypothesis – HEG1 is a flow-sensitive, atheroprotective protein in endothelial cells	20
1.2.2 Aim 1 – Determine whether endothelial HEG1 expression is flow-sensitive.	22
1.2.3 Aim 2 – Determine the role of HEG1 in endothelial function and dysfunction.	22
1.2.4 Aim 3 – Determine the role of HEG1 in the pathogenesis of atherosclerosis.	24
2 Materials and Methods	25
2.1 PCL surgery	25
2.2 scRNA-seq and Gene Array	25
2.3 Hybridization chain reaction (HCR)	25
2.4 Cell culture	26
2.5 In vitro shear stress experiments	27
2.6 qPCR	27
2.7 Western blot	28
2.8 Immunocytochemistry	30
2.9 siRNA knockdown	31
2.10 Endothelial function studies	31
2.11 Plasmid overexpression and viral particle transduction	33
2.12 HEG1^{iECKO} mice	33
2.13 Mouse atherosclerosis studies	34
2.14 Human coronary artery studies	35
2.15 Statistical analyses	37
3 Results	38
3.1 Aim 1 - Determine whether endothelial HEG1 expression is flow-sensitive.	38

3.1.1	Flow controls HEG1 expression and subcellular translocation in endothelial cells	38
3.1.2	Flow-induced HEG1 transcription is promoted by increased chromatin availability and performed by transcription factors KLF2 and KLF4	42
3.2	Aim 2 - Determine the role of HEG1 in endothelial function and dysfunction.	44
3.2.1	HEG1 mediates multiple ULS-induced functional changes in HAECs	44
3.2.2	HEG1 mediates flow-induced KLF2/4 expression by the MEKK3-MEK5-ERK5-MEF2 pathway.....	44
3.2.3	HEG1 controls protein level of MEKK3-inhibitor KRIT1 by co-secretion in response to flow	50
3.3	Aim 3 - Determine the role of HEG1 in the pathogenesis of atherosclerosis.	53
3.3.1	HEG1 ^{iECKO} mice have reduced endothelial KLF2/4 and eNOS expression and increased levels of atherosclerosis	53
3.3.2	Endothelial HEG1 expression is negatively correlated with plaque severity and hypertension in human coronary arteries	58
4	<i>Discussion</i>.....	61
4.1	Summary.....	61
4.2	Conclusion.....	62
4.3	Future Directions	63
5	<i>References</i>.....	66

List of Figures

FIGURE 1.1 DISTURBED FLOW INDUCES ATHEROSCLEROSIS.....	4
FIGURE 1.2 IN VIVO AND IN VITRO MODELS OF D-FLOW-INDUCED ATHEROSCLEROSIS.....	6
FIGURE 1.3 MECHANOSENSORS AND MECHANO-SIGNAL TRANSDUCTION PATHWAYS IN ENDOTHELIAL CELLS	10
FIGURE 1.4 HYPOTHESIS AND SPECIFIC AIMS	23
FIGURE 3.1 HEG1 MRNA EXPRESSION IS REGULATED BY FLOW IN VIVO.	39
FIGURE 3.2 FLOW CONTROLS HEG1 MRNA AND PROTEIN EXPRESSION, AS WELL AS PROTEIN SUBCELLULAR LOCALIZATION IN VITRO	41
FIGURE 3.3 INCREASED CHROMATIN AVAILABILITY AND THE TRANSCRIPTION FACTORS KLF2 AND KLF4 CONTROL FLOW-INDUCED HEG1 EXPRESSION	43
FIGURE 3.4 HEG1 MEDIATES MULTIPLE ULS-INDUCED FUNCTIONAL CHANGES IN HAECs....	45
FIGURE 3.5 HEG1 MEDIATES ULS-INDUCED KLF2/4 EXPRESSION IN HAECs VIA MEKK3-MEK5- ERK5-MEF2 PATHWAY	47
FIGURE 3.6 MEK5 AND ERK5 INHIBITION BLOCKS ULS-INDUCED KLF2/4 EXPRESSION.....	49
FIGURE 3.7 KRIT1 INHIBITS MEKK3-MEK5-ERK5-MEF2 PATHWAY, AND HEG1 MEDIATES ULS- INDUCED SECRETION OF KRIT1	51
FIGURE 3.8 CCM2/2L AND CCM3 INHIBIT KLF2/4 INDUCTION IN ULS.....	52
FIGURE 3.9 EC-SPECIFIC HEG1 KNOCKOUT REDUCES ENDOTHELIAL KLF2/4 EXPRESSION AND INCREASES ATHEROSCLEROSIS IN MICE EXPOSED TO 2 WEEK PCL	55
FIGURE 3.10 HEG1 ^{WT} AND HEG1 ^{IECKO} MOUSE CHARACTERISTICS AND SEX-DEPENDENT ATHEROSCLEROSIS DEVELOPMENT	57
FIGURE 3.11 HEG1 EXPRESSION IS REDUCED WITH INCREASING PLAQUE SEVERITY AND HYPERTENSION IN HUMAN CORONARY ARTERIES	59

List of Tables

<i>TABLE 1.1</i> FLOW-SENSITIVE GENES	18
TABLE 2.1 QPCR PRIMER SEQUENCES.....	29
TABLE 2.2 SIRNA SEQUENCES	32
TABLE 2.3 HUMAN HEART DONOR INFORMATION.....	36

List of Abbreviations

BIX	BIX02189 (MEK5 inhibitor)
CCM	cerebral cavernous malformation disease
CCM2	cerebral cavernous malformation 2 protein (also known as malcavernin or OSM)
CCM2L	cerebral cavernous malformation 2-like protein
CCM3	cerebral cavernous malformation 3 protein (also known as PDCD10)
CM	conditioned media
D-flow	disturbed flow
ECs	endothelial cells
EndMT	endothelial to mesenchymal transition
EndIT	endothelial to immune cell transition
eNOS	endothelial nitric oxide synthase protein
ERK5	extracellular signal-regulated kinase 5 (also known as MAPK7 and BMK1)
HAEC	human aortic endothelial cell
HCR	hybridization chain reaction (also known as HCR RNA-FISH)
HDL	high density lipoprotein
HEG1	heart of glass homolog 1 protein
HEG1^{iECKO}	HEG1 inducible endothelial cell knockout mice
HEG1^{fl/fl}	HEG1 homozygous floxed mice
HEG1^{WT}	HEG1 WT mice (genotype = <i>Cdh5-CreERT2^{+/-};HEG1^{fl/fl}</i>)
IMT	intima-media thickness
KLF2	krüppel-like factor 2 protein
KLF4	krüppel-like factor 4 protein
KRIT1	krev interaction trapped 1 protein (also known as CCM1)
LAD	left anterior descending coronary artery
LCA	left carotid artery
LDL	low-density lipoprotein
LDLR	low-density lipoprotein receptor
MAP	mean arterial pressure
MEF2	myocyte enhancer factor 2 (two forms: MEF2A and MEF2C)
MEK5	mitogen-activated protein kinase kinase 5 (also known as MAP2K5)

MEKK3	mitogen-activated protein kinase kinase kinase 3 (also known as MAP3K3)
ORO	Oil red O dye
OSS	oscillatory shear stress
PCL	partial carotid ligation surgery
Pon	ponatinib (MEKK3 inhibitor)
Rasip1	ras interacting protein 1
RCA	right carotid artery
S-flow	stable flow
ULS	unidirectional laminar shear stress
XMD	XMD8-92 (ERK5 inhibitor)

1 Introduction

1.1 Background

1.1.1 Atherosclerosis

Atherosclerosis is a multifactorial and chronic inflammatory disease of the arteries, in which fibrofatty plaques develop in the arterial wall (1). As advanced plaques develop, the arterial wall stiffens, the arterial lumen narrows, and occasionally plaques rupture, resulting in severe clinical consequences, including myocardial infarction, ischemic stroke, and peripheral arterial disease, which are the leading causes of death worldwide (2).

Dysfunction and inflammation of endothelial cells (ECs) plays a critical role in the initiation and progression of atherosclerosis (3). ECs lining the inner layer of the blood vessels are in direct contact with blood and become dysfunctional and inflamed in response to various risk factors, such as hypercholesterolemia, diabetes, hypertension, smoking, and aging, especially at specific atherosclerosis-prone regions associated with disturbed blood flow. At these sites of endothelial inflammation, circulating monocytes bind to ECs and transmigrate into the sub-endothelial space, becoming macrophages. These regions also show increased permeability to circulating low-density lipoprotein (LDL) cholesterol, which becomes oxidized in the sub-endothelial space and ingested by nearby macrophages, promoting foam cell development and triggering a vicious cascade of inflammation and macrophage accumulation. In addition, vascular smooth muscle cells in these regions transdifferentiate into synthetic phenotypes, migrate to the sub-endothelial layer, and proliferate, contributing to arterial wall thickening. Further, some vascular smooth muscle cells transdifferentiate into foam cells, eventually leading to fatty streaks and fibro-fatty plaques. As plaques

grow outwardly and inwardly, mature, and advance, some plaques rupture, causing major cardiovascular events, such as myocardial infarction and stroke (4; 5).

Although atherosclerotic risk factors such as hypercholesterolemia, hyperglycemia, and hypertension are systemic, plaques preferentially develop in a focal manner in curved and branching regions of the arteries associated with disturbed blood flow. Disturbed flow in these regions is characterized by the delivery of low-magnitude and oscillatory shear stress to the EC surface (6-8). ECs detect various shear stress patterns and magnitudes through mechanosensing receptors (mechanosensors), which translate these mechanical cues into cell signaling (mechanosignal transduction) and subsequent structural and functional responses. Advanced OMICs analyses have demonstrated that flow potently regulates nearly all facets of endothelial biology and pathobiology, from individual molecules and genes to entire cellular structures and functions. Flow regulates EC transcriptomic and epigenomic landscapes in a genome-wide scale *in vivo* and *in vitro*, altering endothelial function, proliferation, death, and differentiation. While stable blood flow, with characteristic high-magnitude, unidirectional laminar shear stress observed in straight, non-branching regions of the vasculature, promotes atheroprotective endothelial homeostasis, disturbed flow promotes pro-atherogenic endothelial responses, including EC dysfunction.

Although lipid-lowering drugs such as statins and PCSK9 inhibitors are highly efficient in reducing blood cholesterol levels and cardiovascular disease burden, atherosclerotic diseases continue to be leading causes of death worldwide, highlighting the need for novel anti-atherogenic drugs targeting non-lipid, pro-atherogenic pathways. In this context, the CANTOS trial demonstrated that the inhibition of vascular inflammation using the IL-1 β inhibitor canakinumab significantly reduced atherothrombotic events in human patients in a non-cholesterol-dependent manner (9). While canakinumab was not FDA-approved due to an increase in fatal infection, the trial demonstrated that targeting an inflammatory pathway could lead to a novel and effective anti-atherogenic therapy.

Similarly, genes, proteins, and pathways regulated by flow (flow-sensitive) that control pro-atherogenic EC dysfunction and inflammation could be promising novel therapeutic targets for atherosclerosis.

1.1.2 Disturbed blood flow induces atherosclerosis

Vascular hemodynamics: The vascular endothelium is in direct contact with blood in the arterial lumen and forms a protective barrier between the blood and the outer vascular wall (10; 11). The vascular endothelium is constantly exposed to hemodynamic forces: normal (transmural) stress from blood pressure, circumferential stress in the arterial wall, and tangential shear stress on the endothelial surface (**Fig. 1.1a**). While transmural pressure and circumferential stress in the vessel wall mainly impact and regulate the medial vascular smooth muscle cells, fluid shear stress is mostly received by ECs, potently regulating their function (12-15).

Shear stress on endothelial cells: Shear stress is the frictional force derived from blood viscosity and flow rate that acts tangentially on the endothelial surface (16; 17). Due to complex vascular geometries and hemodynamic conditions, shear stress levels and directional patterns vary greatly in different regions of the vasculature (17). In straight, non-branching regions of human arteries, inertial forces of blood flow predominate over viscous forces, leading to stable, unidirectional laminar flow (s-flow), which delivers high-magnitude, unidirectional laminar shear stress (ULS; >15 dyne \cdot cm $^{-2}$) to ECs (18). Conversely, in curved and branching regions, viscous forces in the blood predominate over inertial forces, leading to disturbed, multi-directional oscillatory flow (d-flow) that delivers low-magnitude, oscillatory shear stress (OSS; $\sim \pm 4$ dyne \cdot cm $^{-2}$) to the EC surface (16; 19-22). While the terms s-flow and d-flow are typically used for *in vivo* studies, most *in vitro* studies use ULS and OSS to describe the experimental flow conditions to which ECs are exposed. To reduce potential confusion and simplify these interchangeable terms, we will simply use s-flow or d-flow, whenever feasible, in this review. The clinical significance of d-flow is that atherosclerosis preferentially develops

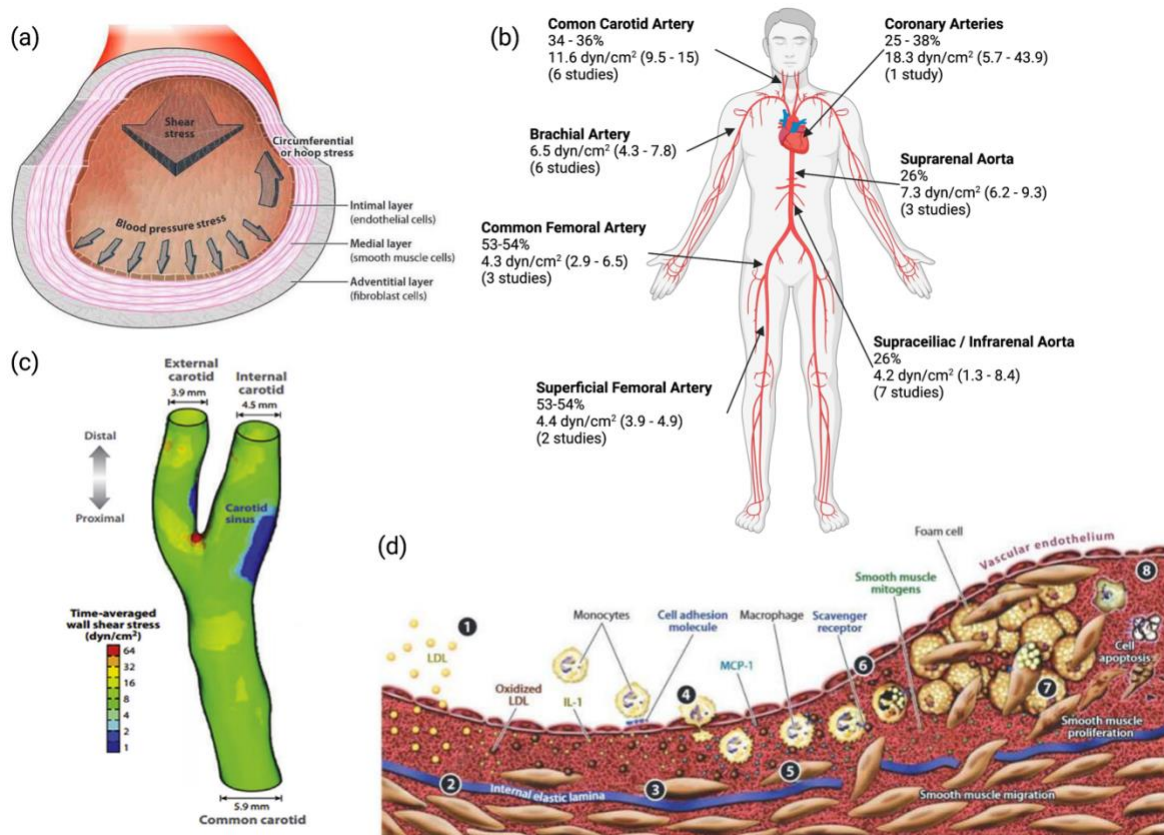


Figure 1.1 Disturbed flow induces atherosclerosis.

(a) Hemodynamic forces experienced by endothelial cells in human arteries. Disturbed flow delivers low-magnitude and oscillatory shear stress. **(b)** Common sites of atherosclerosis development with associated percent prevalence of plaques in middle-aged adults from recent AWHs and PESA studies, and average shear stress levels and ranges from collected literature (23; 24). **(c)** Time-averaged shear stress levels in carotid bifurcation show that the lateral wall of the internal carotid, a common site of atherosclerosis development, experiences low magnitude shear stress from disturbed flow. **(d)** Stages of atherosclerotic plaque development. Figures adapted from Simmons *et al.* (17).

in curved or branching vascular regions exposed to this flow condition. For example, atherosclerotic plaques occur preferentially in the lateral wall of the internal carotid artery at the carotid bifurcation, the lesser curvature of the aortic arch, and the proximal portion of the left anterior descending coronary artery (**Fig 1.1b, c, d**) (23-28).

Animal models of flow-induced atherosclerosis: While clinical observations strongly suggested a correlation between d-flow and sites of atherogenesis, it was not known whether d-flow directly caused atherosclerosis until it was proven by experimental animal studies. The partial carotid ligation (PCL) model and the shear-modifying constrictive carotid cuff model are the two experimental mouse models that directly demonstrated the effect of d-flow, or low flow, on atherosclerosis development (29; 30). In the PCL model, three of the four caudal branches of the left common carotid artery (LCA) are surgically ligated without manipulating the common carotid artery itself. The PCL surgery induces d-flow in the LCA with characteristic low and oscillatory shear stress patterns. In ApoE^{-/-} mice or PCSK9-overexpressing C57BL/6 mice fed a high-fat diet to induce hypercholesterolemia, the PCL surgery causes rapid development of atherosclerosis in the entire length of the LCA within 2 to 3 weeks. Importantly, in this mouse model, the contralateral RCA continues to be exposed to s-flow and does not develop plaque, serving as an ideal control in the same animal (**Fig. 1.2a**) (31). The carotid cuff model uses a shear-modifying cast implanted over a portion of the common carotid artery. The shear-modifying carotid cuff (cast) exposes a portion of the RCA to three different shear regimes and atherosclerosis-development patterns in hypercholesterolemic ApoE^{-/-} mice fed a Western diet: 1) low-magnitude s-flow in the region proximal to the cast causing vulnerable plaque development, 2) high-magnitude s-flow within the casted region with no plaque development, and 3) d-flow in the region distal to the cast that develops stable plaques. This design demonstrates flow-dependent atherosclerosis development within a single carotid artery (**Fig. 1.2b**) (30).

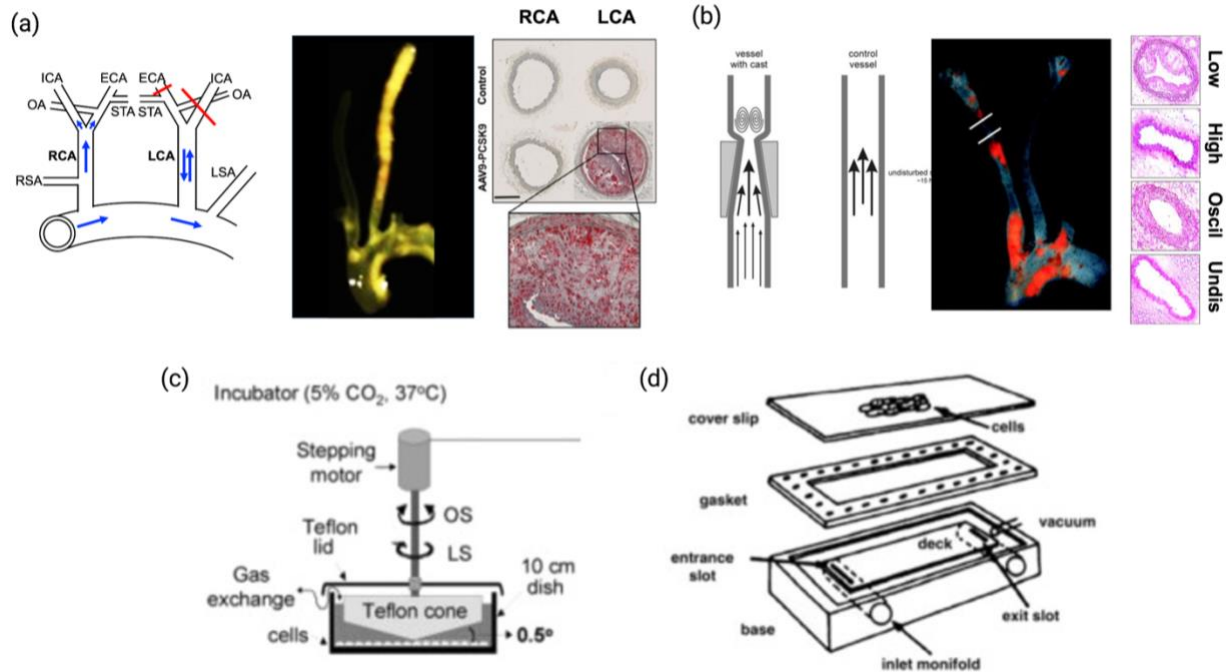


Figure 1.2 *In vivo* and *in vitro* models of d-flow-induced atherosclerosis.

(a) Schematic representation of the PCL model of mouse atherosclerosis. ECA, OA, and ICA are surgically ligated (Red) to induce D-flow and systemic atherosclerosis development in the LCA. RCA: Right common carotid artery, LCA: Left common carotid artery RSA: Right subclavian artery LSA: Left subclavian artery OA: ICA: Internal carotid artery ECA: External carotid artery STA: Superior thyroid artery, OA: occipital artery. Adapted from Nam *et al.* (32). **(b)** Schematic representation of shear-modifying constrictive cuff model. Implanting constrictive cuff on the carotid artery exposes EC to low-magnitude ULS in the proximal region of the cast, high-magnitude ULS within the cast, and OSS in the distal region of the cast. Adapted from Cheng *et al.* (33). **(c-d)** Schematic representations of cone-and-plate viscometer and parallel-plate flow chamber. Rotating Teflon cone and computer-generated hydrostatic pressure exposes ECs to differential shear stress. Adapted from Sucosky *et al.* and Lawrence *et al.*, respectively (34; 35).

Both animal models have been adopted in numerous labs worldwide, providing extremely valuable tools to study flow-dependent endothelial function and atherogenic mechanisms *in vivo*. One major difference between the models is that in the PCL model, atherosclerotic plaques occur throughout the entire length (~1 cm) of the LCA, while the contralateral RCA control remains healthy, providing sufficient amounts of endothelial samples from the LCA and RCA in the same animal to conduct OMICs studies, such as single-cell RNA sequencing or bulk RNA sequencing (15). In addition to these mouse models of d-flow-induced atherosclerosis, the use of zebrafish has emerged as a genetically tractable model to examine early events of atherogenesis (36; 37). Combined with genetic manipulation approaches to reduce blood flow, zebrafish models provide further evidence that d-flow causes atherosclerosis under hypercholesterolemic conditions (28; 38-41). An interesting question is whether d-flow-induced atherosclerosis occurs under other risk factor conditions, such as diabetes and hypertension, independent of hypercholesterolemia.

In vitro flow models: Numerous *in vitro* models of shear stress, including the cone-and-plate viscometer, parallel plate flow chamber, and the microfluidic channel have been developed and were reviewed previously (42; 43). These *in vitro* bioreactors expose ECs to various shear conditions to determine the detailed mechanisms of shear-dependent endothelial function in a well-defined biomechanical environment (**Fig. 1.2c, d**).

1.1.3 Flow potently regulates EC function

ECs *in vivo* are constantly exposed to various hemodynamic conditions, especially shear stress associated with blood flow, which potently regulates nearly all facets of EC function. Flow regulates vascular tone, proliferation, death, differentiation, senescence, metabolism, permeability barrier function, angiogenesis, inflammation, morphology, and matrix remodeling (44). Defining the mechanisms by which s-flow protects endothelial homeostatic function, and d-flow induces

endothelial dysfunction is crucial in understanding the pathogenesis of flow-dependent atherosclerosis, and developing novel therapeutic approaches.

Flow potently regulates permeability barrier function. S-flow protects the endothelial permeability barrier, while d-flow promotes permeability barrier dysfunction (45; 46). Flow regulates EC permeability by promoting tight junction stability via control of occludin expression and attachment to the actin cytoskeleton, as well as control of adherens junction integrity via phosphorylation and degradation of VE-cadherin (47-49).

Flow regulates EC proliferation and apoptotic cell death via multiple mechanisms, including the downregulation of tumor suppressor protein p53 expression and inhibition of the anti-apoptotic kinase Akt (50-53). S-flow induces autophagy through a SIRT1- and FOXO1-dependent pathway, providing a cytoprotective mechanism for ECs (54). D-flow is also known to induce EC senescence through a p53- and SIRT1-dependent mechanism, affecting EC migration and repair mechanisms (55).

Flow also regulates metabolism and redox regulation. Whereas s-flow reduces endothelial glucose uptake, glycolytic gene expression, and metabolic activity, d-flow promotes glycolytic metabolism, causing a markedly different metabolomic profile and increased mitochondrial fission (56-59). D-flow also increases endothelial production of reactive oxygen species (ROS) and oxidative stress (60). This process was shown to be mediated by bone morphogenic protein 4 (BMP4), which induces increased superoxide production via the NADPH oxidases and eNOS uncoupling-dependent mechanisms (20; 61; 62). Endothelial ROS generation in response to d-flow increases vascular oxidative stress and LDL oxidation in the context of atherosclerosis and hypertension (62-64).

D-flow potently induces endothelial inflammation and transdifferentiation of ECs, which play critical roles in the initiation and progression of atherosclerosis. D-flow induces endothelial inflammation by increasing the expression of endothelial adhesion molecules (VCAM1, ICAM1, and

E-selectin), which mediate monocyte adhesion to ECs. Activation of the nuclear factor- κ B (NF- κ B) is a critical pathway by which d-flow induces inflammation (65). In addition, d-flow also induces the expression of cytokines and chemokines IL-1, IL-6, and CCL5 (65; 66). Recent studies reveal that flow can induce the transdifferentiation of ECs to mesenchymal cells (EndMT) and immune-like cells (EndIT) (15). While the pathophysiological importance of EndMT in d-flow-induced atherosclerosis has been demonstrated, the validation and significance of EndIT in atherosclerosis remains to be determined (67). Increased endothelial turnover under d-flow conditions also coincides with increased transcription of angiogenic genes and increased neovascularization (68).

Morphologically, ECs adopt an elongated, fusiform shape and align to the direction of flow under s-flow conditions, while ECs under d-flow or no-flow static conditions adopt a polygonal, “cobblestone” shape without uniform alignment (22; 69-71). These morphological changes are accompanied by actin cytoskeleton remodeling from a pattern of bands encircling the periphery of the cell to a pattern of thick, central stress fibers aligned in the direction of shear stress (72; 73). These cytoskeletal changes alter intercellular stress and cellular traction forces, affecting subsequent cellular strain and status (74; 75). In addition, shear stress affects subcellular structural changes, such as nuclear shape and relocation of the Golgi apparatus toward the upstream flow direction (76; 77).

1.1.4 Mechanosensors and mechanosignal transduction in endothelial cells

ECs transduce flow signals into intracellular changes through the processes of mechanosensing and mechanosignal transduction. ECs recognize fluid shear stress through mechanosensors located in the apical and basal surfaces of the cell, the cell-cell junctions, and intracellularly (**Fig. 1.3**). On the apical surface, plasma membrane proteins, including the Piezo1 and P2X4 purinoreceptor cation channels, NOTCH1, protein kinases, G-protein coupled receptors (GPCRs), plexin D1, and membrane structures like caveolae, the glycocalyx, and primary cilia serve as

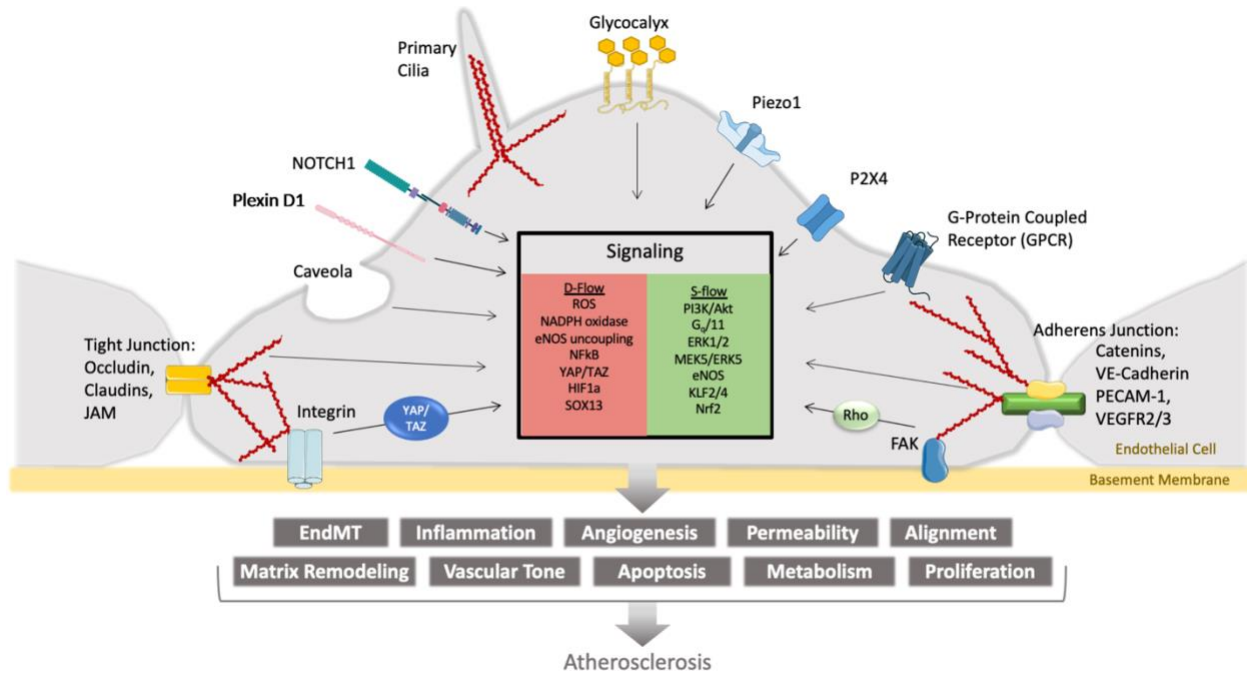


Figure 1.3 Mechanosensors and mechano-signal transduction pathways in endothelial cells.

The apical surface of the cell contains protein mechanosensors, such as Plexin D1, NOTCH1, Piezo1, P2X4 and GPCRs like GPR68, as well as mechanosensitive cell structures, like caveolae, primary cilia and the glycocalyx. Cell-cell junctions contain the mechanosensory complex comprised of VE-cadherin, PECAM1 and VEGFR2/3. The basal surface of ECs contain integrin mechanosensors. Mechano-signal transduction pathways include the PI3K/Akt pathway, ERK1/2 pathway, YAP/TAZ pathway, and the Rho signaling pathway. Many mechano-signal transduction pathways result in transcription factor activation like KLF2/4, NF-κB and HIF-1α. Figure adapted from Demos *et al.* (78).

mechanosensors. PECAM1, VE-cadherin, and VEGFR2 form the junctional mechanosensory complex in the cell-cell junction, which mediates integrin activation, cellular alignment, and endothelial nitric oxide synthase (eNOS) activation in response to s-flow via PI3K/Akt signaling (74; 79; 80). Plexin potentially in connection with the junctional mechanosensory complex, mediates flow-dependent atherosclerosis development by regulating calcium uptake, phosphorylation of VEGFR2, Akt, eNOS, and ERK1/2, as well as induction of the major flow-sensitive transcription factors, KLF2 and KLF4 (81). Piezo1 is an inward-rectifying, calcium channel that opens in response to mechanical force in many cell types (82). In ECs, Piezo1 mediates shear stress magnitude-dependent increases in calcium levels, influencing flow-induced, anti- and pro-atherogenic responses, such as cell alignment (83-85). Notch1 mediates s-flow-induced cellular alignment, suppression of proliferation, and cell-cell junctional integrity, as well as atherosclerosis (86). These effects were suggested to be controlled by tension-induced Notch1 signaling and modulation of intracellular calcium levels. GPCRs, such as the proton-sensing GPR68, undergo conformational changes in response to flow in ECs mediating shear-induced calcium influx (87; 88).

In addition to the membrane protein mechanosensors, several apical membrane-associated EC structures, such as the glycocalyx, primary cilia, and caveolae, have been suggested to serve as mechanosensors (89-92). On the basal surface of ECs, flow induces conformational activation and expression changes in extracellular matrix (ECM)-binding integrin mechanosensors (80; 93). S-flow activates the $\alpha v\beta 3$ integrin, causing increased ECM binding and inactivation of downstream Rho signaling. In addition, the actin cytoskeleton in the cytosol has been shown to serve as a mechanosensory structure (94).

Upon mechanosensing in ECs, flow activates numerous early-to-intermediate (seconds to minutes) cell signaling pathways that lead to long-term (>hour) atheroprotective or pro-atherogenic conditions. However, it is important to note that both pro-atherogenic d-flow and atheroprotective s-

flow often activate many of the same early-to-intermediate signaling pathways, especially in *in vitro* studies. For example, s-flow transiently activates NF- κ B without leading to long-term endothelial inflammation, whereas d-flow induces persistent NF- κ B activation resulting in endothelial inflammation. The mechanisms that distinguish these flow-pattern-dependent activation pathways, especially *in vitro*, are not well understood and remain as critical knowledge gaps to be filled. This uncertainty is due in part to a common experimental strategy of conducting *in vitro* studies with ECs cultured under no-flow conditions that are suddenly subjected to s-flow or d-flow exposure. Under these conditions, early-to-intermediate responses may overlap with common adaptive changes in response to altered mechanical cues indifferent of flow patterns and magnitudes. With this caveat in mind, we review the literature that provides crucial knowledge in understanding flow-dependent EC mechanosignal transduction pathways.

Piezo1: Piezo1 mediates both atheroprotective and pro-atherogenic flow-dependent EC responses (95; 96). S-flow induces eNOS activation, producing the atheroprotective and vasorelaxant NO from ECs. Upon Piezo1 mechanosensing, s-flow induces intracellular calcium influx leading to ATP release, eNOS activation, NO production, and subsequent vasodilation (83; 97). Studies further showed that the Piezo1-induced ATP effect was mediated by the P2Y₂ and G α q/11 pathway, activating Akt and eNOS in sequence (98; 99). In contrast, Piezo1 can also mediate pro-atherogenic endothelial responses of d-flow. D-flow stimulates NF- κ B activity and endothelial inflammation via Piezo1-G α q/11-mediated integrin activation, which in turn activates the focal adhesion kinase (FAK). Endothelial-targeted deletion of Piezo1 in LDL receptor (LDLR) knockout mice inhibited atherosclerotic plaque development in d-flow regions, suggesting a pro-atherogenic role of endothelial Piezo1 (100).

Plexin D1: Plexin D1 is another mechanosensor that responds to both s-flow and d-flow, mediating both atheroprotective and pro-atherogenic responses, respectively. Plexin D1 knockdown

inhibits atheroprotective EC signal transduction pathways, such as eNOS activation, cell alignment, and KLF2 and 4 expression in response to s-flow. Interestingly, Plexin D1 knockout also prevents pro-atherogenic EC inflammation responses, including VCAM1 and MCP1 expression in response to d-flow. EC-specific knockout of Plexin D1 prevented atherosclerosis development in d-flow regions, while exacerbating plaque development in s-flow regions. These results suggest that Plexin D1 is a mechanosensor with dual functions depending on blood flow patterns.

Junctional mechanosensory complex: S-flow stimulates eNOS through the mechanosensory complex formed by PECAM1, VE-cadherin, and VEGFR2 or VEGFR3, which activates the PI3K and Akt pathway (74; 101). S-flow induces integrin $\alpha v \beta 3$ integrin activation and NF- κ B activation through the mechanosensory complex. Interestingly, however, PECAM1 knockout prevents endothelial inflammation and atherosclerosis in d-flow arterial regions in mice (74; 102). This suggests that PECAM1 is a mechanosensor mediating pro-atherogenic effects of d-flow *in vivo*.

Integrins: Integrin activation in response to s-flow inactivates Rho through Rho-like GTPase signaling (103; 104). This inactivation controls YAP phosphorylation (at S127 and S381) in the cytoplasm to maintain an atheroprotective EC phenotype (105). These interactions further activate Rac, leading to the assembly of the junctional mechanosensory complexes (106). Additionally, cell division cycle 42 is polarized and activated in an integrin-dependent manner and subsequently regulates the polarity of the microtubule organizing center (107; 108). Under d-flow conditions, the cooperation between RGD-binding integrins (including $\alpha 5 \beta 1$ and $\alpha v \beta 3$) and fibronectin has also been shown to drive pro-inflammatory signal transduction, involving NF- κ B, PAK, and YAP nuclear translocation (103; 109-111).

Flow-sensitive transcription factors: Thus far, we have discussed mechanosignal transduction pathways occurring in an early-to-intermediate time scale, mediated by specific mechanosensors in response to flow in ECs. These relatively acute responses lead to the regulation of

downstream, long-term responses, including activation of transcription factors and transcriptional co-activators, such as KLF2 and 4 (KLF2/4), NF- κ B, HIF-1 α , YAP/TAZ, and SOX13, which regulate gene expression profiles and cell function (78). KLF2/4 are two of the most flow-sensitive master transcription factors regulating the expression of genes that control anti-atherogenic pathways, including vasodilation, anti-thrombotic and anti-inflammatory pathways induced by s-flow (112-116). KLF2 diminishes pro-atherogenic gene expressions by competing with NF- κ B for transcriptional cofactor CBP/p300 and promoting translocation of nuclear respiratory factor 2 (Nrf2) (117-119). S-flow increases KLF2 transcription by sequentially activating the members of the MAP kinase family MEKK3, MEK5, and ERK5, which in turn activates the MEF2A/C (120). In contrast, d-flow inactivates the ERK5 pathway, leading to the inhibition of KLF2 expression. In addition, KLF2 expression is controlled by the flow-dependent microRNA, miR-92a (17; 121-127).

NF- κ B is a well-recognized transcription factor activated by flow. Nuclear translocation and activation of NF- κ B is increased transiently by s-flow and persistently by d-flow (128; 129). Target genes of NF- κ B include VCAM-1, ICAM-1, E-selectin, HIF-1 α , and numerous cytokines, all of which play a critical role in atherosclerosis (130-132). HIF-1 α is another pro-atherogenic transcription factor activated by d-flow (133-135). HIF-1 α induces the expression of glycolytic enzymes such as HK2, PFKFB3, and PDK-1 (136). Furthermore, YAP and TAZ, the well-known transcriptional co-activators induced by the Hippo signaling pathway that are involved in organ growth, development, and various diseases such as cancer and atherosclerosis, are regulated by flow (137-139). D-flow induces YAP/TAZ nuclear translocation and activation, leading to endothelial inflammation, cytoskeletal remodeling, and atherosclerosis (137-139). Recently, SOX13 was identified as a novel flow-sensitive transcription factor. The loss of SOX13 by d-flow leads to a profound induction of

pro-inflammatory cytokines and chemokines, including CCL5 and CXCL10, resulting in endothelial inflammation (140).

1.1.5 OMICs approaches to determine flow-sensitive endothelial genes, proteins, and pathways

OMICs-based analyses have become standard approaches to determining changes in ECs in response to various flow and disease conditions. Unlike traditional reductionist approaches studying one or few candidate genes or proteins at a time, the astonishing advancement in OMICS technologies and computational bioinformatics have made it possible to determine changes in genes, proteins, and metabolites in a genome-, epigenome-, proteome-, and metabolome-wide scale, using a relatively small amount of samples, often at a single-cell resolution. The application of these approaches using *in vitro* and *in vivo* models has generated a plethora of flow-dependent transcriptomic, epigenomic, proteomic, and metabolomic datasets in ECs and blood vessels under healthy and disease conditions (15; 141-145).

Early transcriptomic studies used bulk RNA and microRNA samples from pooled cultured ECs and animal tissues to conduct microarrays and RNA sequencing analyses. These datasets identified numerous unexpected flow-sensitive genes, microRNAs, and non-coding RNAs, generating wide-ranging novel hypotheses regarding their various roles in EC function and atherosclerosis (17; 42; 78). Numerous flow-sensitive genes, including KLF2, BMP4, DNMT1, KLK10, TXNDC, ZBTB46, thrombospondin1, JMJD2B, semaphorin7A, PPAP2B, miR-712, and miR-95a were identified from these bulk RNA studies and subsequently validated as reviewed elsewhere (17; 42; 146; 147). Recently, kallikrein-related peptidase 10 (KLK10) was identified as one of the most flow-sensitive genes from a gene array study using the mouse PCL model (141). KLK10 expression is increased by s-flow, but nearly lost by d-flow in ECs *in vitro*, mouse arteries *in vivo*, and human coronary

arteries with advanced atherosclerotic plaques. Once produced, KLK10 is secreted into circulating blood *in vivo* or conditioned medium *in vitro* and serves as an anti-inflammatory and permeability-barrier-protective protein. Interestingly, KLK10, a member of the KLK serine/threonine protein kinase family, lacks inherent protease activity, but its anti-inflammatory and permeability-barrier-protective function are mediated by a protease activated receptor (PAR) 1 and 2-dependent pathway. Further, recombinant KLK10 injection via tail-vein or ultrasound-guided delivery of KLK10 expression vector to the carotid endothelium prevented endothelial inflammation and atherosclerosis development in mice, demonstrating the proof-of-principle that the flow-sensitive proteins such as KLK10 could be used as novel anti-atherogenic therapeutics (148; 149).

Flow induces epigenome-wide changes in ECs, as revealed by a DNA methylome study using reduced representation bisulfite sequencing with bulk genomic DNA samples combined with a microarray study of bulk RNA samples in mouse carotid arteries, following the partial carotid ligation surgery (15). This DNA methylome study, along with studies from other investigators showed that d-flow regulates DNA methylation patterns via DNA methyltransferase isoforms, DNMT 1&3 (142; 150; 151). Further studies showed that genetic deletion or pharmacological inhibition of DNMT1 prevented endothelial inflammation and atherosclerosis development in ApoE^{-/-} mice, demonstrating that flow-sensitive epigenomic modifications could serve as anti-atherogenic therapeutic targets.

Proteomics studies using advanced mass spectrometry have identified numerous flow-sensitive proteins differentially expressed or post-translationally modified in ECs in response to flow (17; 147; 152; 153). Flow alters the expression level of hundreds of proteins in cell lysates or secreted media (secretome), including BMP6 and endothelin-1 in ECs. An interesting study was conducted to determine proteome-wide S-sulfhydration changes of reactive cysteines (S-sulfhydrome) *in vitro* and *in vivo*. Hundreds of flow-sensitive S-sulfhydrated proteins were identified, including integrins that play an important role in the flow-dependent vascular relaxation response (154). A metabolomics study

using plasma samples of ApoE^{-/-} mice subjected to the PCL surgery showed that d-flow induces significant changes in hundreds of metabolites, including sphingomyelin and the amino acids methionine and phenylalanine (58). However, the causal effects of flow-dependent changes in metabolites have not been clearly defined yet *in vivo* and warrant further investigation. Targets identified by OMICs approaches and their roles in endothelial dysfunction and atherosclerosis are summarized in **Table 1.1**.

1.1.6 Therapeutic implications of flow-sensitive genes, proteins, and pathways in atherosclerosis

As discussed in the introduction, the CANTOS trial demonstrated that targeting a non-lipid pathway, such as an inflammatory pathway, could be an effective anti-atherogenic therapy. We propose that flow-sensitive genes, proteins, and pathways in ECs that regulate FIRE, such as endothelial inflammation, EndMT, and EndIT, could be promising novel anti-atherogenic targets. In support of this notion, our transcriptomic study conducted in the mouse PCL model of atherosclerosis showed that both statins and blood flow regulate hundreds of genes that are remarkably distinct from each other. This result suggests that flow and cholesterol pathways play distinct roles in atherosclerosis, highlighting the rationale for targeting flow-sensitive molecules (genes, proteins, and signaling molecules) as a complementary therapeutic approach. Two therapeutic strategies are conceivable: 1) stimulating or increasing s-flow-induced atheroprotective molecules, or 2) inhibiting d-flow-induced pro-atherogenic molecules using small molecules, recombinant proteins, or gene therapies delivered in a systemic or targeted manner. Several s-flow induced molecules are promising anti-atherosclerotic targets. KLF2/4 account for >50% of all s-flow induced gene transcription and affect nearly all facets of atheroprotective responses in ECs. Given their dominant importance, numerous strategies to stimulate KLF2/4 expression have been proposed. Statins are a well-known

Table 1.1 Flow-sensitive genes

Protein-coding genes			
Effect	Protein	Shear	Roles
Anti-Atherogenic	eNOS	ULS up	Nitric oxide production and maintenance of vascular tone
	KLF2	ULS up	Anti-oxidative, antithrombotic, Vascular integrity/identity
	KLF4	ULS up	Anti-oxidative, antithrombotic, Vascular integrity/identity
	Mn-SOD	ULS up	Superoxide dismutase
	EC-SOD	ULS up	Superoxide dismutase
	TIMP3	ULS up	MMPs, ADAMs, ECM degradation
	PPAP2B	ULS up	Regulated by KLF2 and miR-92, anti-inflammatory
	ZBTB46	OSS down	EC Quiescence
	BMPR2	ULS up	Smad, NF κ B, cytoskeleton
	Nrf2	ULS up	Antioxidant Responsive Element (ARE)
	IL10	ULS up	Inflammation
	SOX13	ULS up	Inflammation
	CTNND1	ULS up	Cell adhesion
	MMP1	ULS up	Cell death
Pro-Atherogenic	MCP-1	OSS up	Immune response
	VCAM1	OSS up	Immune response, cell adhesion
	ICAM-1	OSS up	Immune response, cell adhesion
	NF κ B	OSS up	Transcription, cell survival
	NADPH Oxidase	OSS up	Reactive oxygen species
	MMPs	OSS up	Matrix degradation
	p53	OSS up	Apoptosis
	GADD45	OSS up	Growth and proliferation
	p21	OSS up	Growth and proliferation
	ERK1/2	OSS up	Growth and proliferation
	TSP-1	OSS up	Arterial stiffening
	Sema7A	OSS up	β 1 integrin, FAK, MEK1/2, NF κ B, THP-1
	HIF1 α	OSS up	PFKFB3, glycolysis enzymes (hexokinase 2 [HK2], enolase 2), and glucose transporters (glucose transporter 1, glucose transporter 3), NF κ B, Cezanne
	P2X7	OSS up	ATP-dependent p38 signaling
JMJD2B	ULS down	SMC phenotype	

	YAP/TAZ	OSS up	CTGF, CYR61, JNK, Caveolae-associated proteins	
	Hand2	OSS up	lncRNAs, angiogenesis, cardiovascular development	
	TXNDC5	OSS up	Vascular tone	
	GPX-3	OSS up	Oxidative stress	
Non-coding genes				
Type	ncRNA	Shear	Target genes	Roles
miRNA	miR-10a	s-flow up	MAP3K7, β -TRC	Inflammation
	miR-19a	ULS up	Cyclin D1, HMGB1, HBP1	Proliferation
	miR-23b	ULS up	E2F1, FoxO4	Proliferation & SMC phenotype
	miR-27b	ULS up	SEMA6A, SEMA6D, SPRY2, DLL4, Flt1, TGF β	Angiogenesis, EC differentiation, vessel integrity
	miR-101	ULS up	mTOR, Cul3, ABCA1	EC proliferation, angiogenesis
	miR-143/145	ULS up	ELK1, KLF4, CAMK2d, SSH2, PHACTR4, FL1	Inflammation, VSMC phenotype switching
	miR-92a	OSS up	KLF2, KLF4, ITGA5, SIRT1, CXCL1, PPABP2B	EC inflammation, angiogenesis
	miR-205	OSS up	TIMP3	EC inflammation and permeability
	miR-663	OSS up	KLF2, KLF4, SOCS5, MYOCD, Elk-1, VEGF, ATF4	EC inflammation, VSMC phenotype switching
	miR-712	OSS up	TIMP3	EC inflammation and permeability
	miR-21	NA	PTEN, BCL2, PPAR α	EC inflammation and apoptosis
	miR-126	NA	FOXO3, BCL2, IRS1, Dlk1, HMGB1, VCAM1, CCL2, LRP6	EC proliferation, inflammation, angiogenesis
	miR-155	NA	Bcl6, SOCS-1, MYLK, NOS3,	EC inflammation, migration, proliferation
lncRNA	MALAT1	ULS up	NA	EC proliferation, angiogenesis, migration
	MANTIS	ULS up	NA	Angiogenesis
	LINC00341	ULS up	NA	Inflammation
	LISPR1	ULS up	NA	EC migration, angiogenesis
	STEEL	ULS down	NA	Angiogenesis

inducer of KLF2 expression in cultured ECs, however whether they also induce KLF2/4 expression *in vivo* under flow-condition has been disputed given the potent effect of flow (114; 155-157). Betulinic acid has also recently been shown to induce KLF2 expression, as well as expression of its critical target gene eNOS, via the upstream ERK5/MEF2C pathway (158). Piezo1 agonists (Yoda1, Jedi1, or Jedi2) or antagonists (salvianolic acid B) have been shown to modify KLF2/4 expression (159-161). However, given the dual atheroprotective and proatherogenic roles of Piezo1, drugs targeting this receptor would require substantial safety and specificity studies in order to be used as atherosclerosis therapies. The use of recombinant KLF10 or targeted overexpression of KLF10 as an anti-atherogenic therapy was discussed above.

Inhibition of d-flow-induced molecules is a promising anti-atherosclerosis strategy. Pharmacologic inhibition of d-flow-induced HIF-1 α using PX-478 small molecule inhibitor was recently shown to reduce atherosclerosis in mice (135). Inhibition of d-flow-induced microRNAs, including the antagomiRs of miR-712, miR-205, or miR-92a, effectively reduced atherosclerosis development in mice as well (162-164). The inhibitor 5-aza-2'-deoxycytidine inhibits the d-flow-induced DNMT activity and atherosclerosis in a mouse model of disease (142). There are numerous flow-sensitive genes, proteins, and pathways, including NF- κ B, YAP/TAZ, and BMP4, as well as specific inhibitors, drugs, or RNA therapeutics suitable for further investigation, but research regarding therapeutic strategies targeting flow-induced atherogenesis has been limited. Developing approaches to overcome this limitation is a major research area to be developed.

1.2 Hypothesis and Specific Aims

1.2.1 Hypothesis – HEG1 is a flow-sensitive, atheroprotective protein in endothelial cells

To understand the role of disturbed flow in the pathogenesis of atherosclerosis, our laboratory seeks to understand the ways in which disturbed blood flow affects vascular endothelial cells, and how

these endothelial responses lead to atherosclerosis. Recently, using the partial carotid ligation mouse model, in which branching arteries from the left carotid are blocked in order to elicit disturbed blood flow in the artery and rapidly induce atherosclerosis, our laboratory identified a novel mRNA transcript that is downregulated in endothelial cells of the atherosclerotic left carotid as compared to the healthy right carotid (32; 165). This mRNA codes for heart of glass homolog 1 (HEG1), a single pass transmembrane glycoprotein that is expressed in vascular endothelial cells and is known to be essential for cardiovascular development and endothelial cell-cell junctional integrity.

Though relatively little has been published on HEG1, it is clear that HEG1 is an important endothelial protein. HEG1 is a single-pass transmembrane glycoprotein primarily expressed in endothelial cells, which possesses extracellular EGF-like domains and a conserved intracellular domain (166; 167). HEG1 was first identified in zebrafish and shown to be essential for cardiovascular development (168). HEG1 knockout zebrafish embryos displayed a lethal phenotype in which myocardial cells failed to grow in concentric layers around the endocardium, leading to massively enlarged hearts with monolayers of myocardium that failed to contract and pump blood (167). HEG1 knockout mice were shown to also have a lethal phenotype in which the porous endocardium allows blood to leak through the walls of the heart. Endothelial cell junctions are degraded in HEG1 KO mice such that blood leaks into the alveoli of the lungs and lymph seeps out of intestinal lymphatic vessels (166). HEG1 has also been shown to have two binding partners on its intracellular C-terminal domain: krev interaction trapped protein 1 (KRIT1) and ras interacting protein 1 (Rasip1). KRIT1 has many binding partners and connected signaling pathways, and is known to be mutated in cases of familial cerebral cavernous malformation (169-173). HEG1 binding to Rasip1 has been shown to be involved in stabilization of endothelial cell-cell junctions via inhibition of the RhoA/Rock signaling pathway (169; 170; 174).

Our preliminary data suggests that HEG1 mRNA and protein is consistently and robustly downregulated by disturbed flow *in vivo*. A recent study on HEG1 in zebrafish showed similar findings. As HEG1 knockout is known to cause lethal phenotypes in zebrafish and mice, local downregulation of HEG1 in vascular endothelial cells exposed to disturbed flow likely has pathological effects. **Therefore, we hypothesize that the downregulation of HEG1 by disturbed flow causes endothelial dysfunction, which contributes to the development of atherosclerosis (Fig. 1.4).** To test this hypothesis, we propose three aims.

1.2.2 Aim 1 – Determine whether endothelial HEG1 expression is flow-sensitive.

To determine whether HEG1 is flow-sensitive, we will first search our recent scRNAseq, scATACseq, and gene array datasets from mouse PCL carotid endothelial cell lysate samples for HEG1 mRNA levels. Additional PCL studies will be performed and specifically assessed for HEG1 mRNA expression changes. Additionally, *in vitro* validation of flow-sensitivity will be performed using the cone and plate viscometer shear system with human aortic endothelial cells (HAECs) and HEG1 mRNA and protein expression, as well as HEG1 protein subcellular localization will be assessed.

1.2.3 Aim 2 – Determine the role of HEG1 in endothelial function and dysfunction.

To evaluate the function of HEG1, we will both overexpress and knock down HEG1 in HAECs using a HEG1 plasmid and HEG1 siRNA, respectively. These HAECs, with either elevated or reduced levels of HEG1, will be used to determine the protein's role in endothelial alignment, inflammation, endothelial-mesenchymal transition (EndMT), migration, permeability, proliferation and tube formation. We will also use HAECs to determine whether HEG1 affects these mechanisms through its intracellular binding partners.

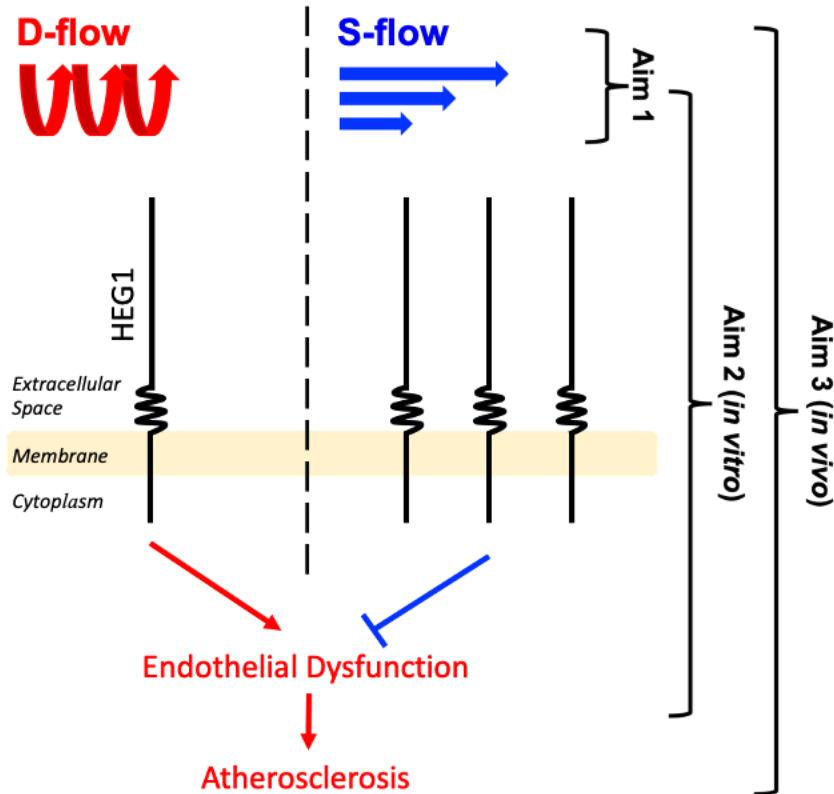


Figure 1.4 Hypothesis and Specific Aims

We hypothesize that low HEG1 expression in disturbed flow (d-flow) conditions leads to endothelial dysfunction and atherosclerosis. In contrast, high levels of HEG1 expression in stable flow (s-flow) conditions prevent endothelial dysfunction and thereby atherosclerosis. Aim 1 is to determine whether HEG1 is regulated by flow. Aim 2 is to determine the role of HEG1 in endothelial function and dysfunction using *in vitro* functional and mechanistic studies on cultured HAECs. Aim 3 is to determine the role of HEG1 in the pathogenesis of atherosclerosis *in vivo* using mice.

1.2.4 Aim 3 – Determine the role of HEG1 in the pathogenesis of atherosclerosis.

We will test the role of HEG1 in atherosclerosis using inducible, endothelial-specific HEG1 knockout mice (HEG1^{ieCKO}), developed by our laboratory. These HEG1^{ieCKO} mice will be injected with AAV-PCSK9 to induce hypercholesterolemia and then subjected to partial carotid ligation surgery to rapidly elicit atherosclerosis. Markers of endothelial dysfunction and atherosclerosis will be studied. We hypothesize that reduced HEG1 will weaken endothelial barrier function and induce more severe atherosclerosis phenotypes.

Addressing these aims will shed light on the role of HEG1 in endothelial biology and the mechanisms through which downregulation of HEG1 by disturbed flow leads to endothelial dysfunction. Knowledge of these mechanisms will reveal novel therapeutic targets for the treatment of atherosclerosis.

2 Materials and Methods

2.1 PCL surgery

All animal studies were approved by the Emory University Institutional Animal Care and Use Committee, and conducted in accordance with federal guidelines and regulations. Prior to partial carotid ligation (PCL) surgery, hypercholesterolemia was induced by treating mice with AAV8-PCSK9 via tail-vein injection, as well as initiating high fat diet, as described previously (32). PCL were performed by ligating 3 of 4 caudal branches (left external carotid, left internal carotid, and left occipital artery were ligated, while leaving the superior thyroid artery intact) of the left common carotid artery (LCA) in anesthetized mice while leaving the contralateral right common carotid artery (RCA) unperturbed. Development of d-flow in the LCA was confirmed by ultrasonography, as described previously (165). Following PCL surgery, mice continued to be fed a high fat diet, and were sacrificed from 1 day to 4 weeks post-ligation, as indicated in the corresponding figures.

2.2 scRNA-seq and Gene Array

scRNA-seq and gene array analysis of *Heg1* mRNA in PCL-exposed mouse RCAs and LCAs was performed as described previously (175; 176).

2.3 Hybridization chain reaction (HCR)

Segments of LCA/RCA and abdominal aorta were isolated and fixed with 4% paraformaldehyde solution (PFA) (Santa Cruz Biotechnology #sc-281692). Hybridization chain reaction RNA-fluorescence in situ hybridization (HCR RNA-FISH) was performed by using custom-designed mouse HEG1 probes (Molecular instruments, CA) to determine HEG1 mRNA levels. Chain reaction specific to the initiator sequence of the probe was performed using fluorescence-conjugated

amplifiers (Molecular instruments, CA). VE-cadherin (1: 500, Ab205336) and nuclei (Hoechst 33342, Thermofisher, MA) was fluorescently labeled to determine changes in endothelial HEG1 mRNA. Following whole-mount HCR assay, the aortic lumen was anatomically exposed *en face* for confocal fluorescence imaging (Zeiss LSM 800, Germany) as previously described (148). Each optical section was projected in the visualization plane where each pixel displayed maximum intensity. Raw confocal images were post-processed with custom-written MATLAB algorithm (MathWorks, MA), ImageJ and Fiji (NIH, MD) to reduce autofluorescence and enhance image contrast. Numbers of individual chain reaction in post-processed images were analyzed by using ImageJ (NIH, MD).

2.4 Cell culture

HAECs (Cell Applications #304-05a) were cultured in a complete medium consisting of MCDB 131 (Corning #15-100-CV), 10% fetal bovine serum (FBS) (R&D Systems #S11550), 1% penicillin-streptomycin (Gibco #15140-122), 1% L-glutamine (Gibco #25030-081), 1% endothelial cell growth supplement (ECGS) from bovine brain extract, 50 µg/mL L-ascorbic acid (Sigma #A5960), 1 µg/mL hydrocortisone (Sigma-Aldrich #H088), 10 ng/mL epidermal growth factor (EGF) (STEMCELL Technologies #78006), 2 ng/mL insulin-like growth factor 1 (IGF-1) (R&D Systems #291-G1), 2 ng/mL fibroblast growth factor (FGF) (ProSpec #cyt-218-b) and 1 ng/mL vascular endothelial growth factor (VEGF) (BioLegend #583706) (177). HAECs were cultured on gelatin-coated (Sigma #G1890) dishes and used for experimentation between passages four and eight. HEK 293T cells were cultured in a complete medium consisting of DMEM (Corning #15-013-CV), 10% FBS, 1% penicillin-streptomycin and 1% mL L-glutamine. Both cell types were cultured in humidified incubators at 37 °C and 5% CO₂, with media changes every three days.

2.5 In vitro shear stress experiments

Shear stress was delivered to HAECs using two devices: cone and plate viscometer and ibidi pump system. The cone and plate viscometer was used for the majority of *in vitro* shear experiments, while the ibidi pump system was used exclusively for the permeability study. For the cone and plate viscometer experiments, custom-made Teflon cones controlled by stepping motors were inserted into 11 mL complete HAEC media overlying HAECs grown to confluency on gelatin-coated 100 mm tissue culture dishes (Falcon #353003). Based on the wall shear stress equation, cone rotation speeds were calculated in order to deliver either unidirectional laminar shear stress (ULS, +15 dyn/cm²) mimicking s-flow, or oscillatory shear stress (OSS, +5/-4 dyn/cm² at 1 Hz) mimicking d-flow. For the ibidi pump system experiments, HAECs grown to confluency on gelatin-coated μ -Slide I^{0.4} Luer ibiTreat channels (ibidi #80176) in complete HAEC media were exposed to either ULS or OSS using the ibidi pump system (ibidi #10902) as per the manufacturer's instructions. All cone and plate viscometer and ibidi pump system experiments were performed in humidified incubators at 37 °C and 5% CO₂. For both experimental setups, static control samples prepared in the same manner as the ULS- and OSS-exposed samples were left in the same incubator during the duration of shear stress exposure. Cells located in the center of the 100 mm dishes used for cone and plate viscometer experiments were excluded from analysis, as desired shear stress is calculated only for the perimeter of dish.

2.6 qPCR

Cells were lysed using QIAzol lysis reagent (Qiagen #79306). EC-enriched vascular lysates were obtained by carotid or thoracic aorta QIAzol flushing, as described previously. RNA was isolated from QIAzol lysates using Direct-zol RNA Miniprep Kit (Zymo Research #R2052) for *in vitro* samples and miRNeasy Mini Kit (Qiagen #217084) for *in vivo* samples. cDNA synthesis was performed using

High Capacity cDNA Reverse Transcription Kit (Applied Biosystems #4368813), and qPCR was performed using PerfeCTa SYBR Green FastMix (QuantaBio #95073-05K) on the StepOnePlus Real-Time PCR System (Applied Biosystems #4376600). 18S ribosomal RNA was analyzed as a loading control and analyses were performed using either the $\Delta\Delta C_t$ method or by calculating transcripts per 1 million 18S (TPM). Primer information is listed in **Table 2.1**.

2.7 Western blot

Cells were lysed using RIPA buffer (Boston BioProducts #BP-115) supplemented with cComplete Mini protease inhibitor cocktail (Roche Diagnostics GmbH #11836153001) and phosphatase inhibitor cocktail 1 (Sigma #P2850). Conditioned media samples were centrifuged to remove detached cells, and the resulting supernatants concentrated via size-filtration using either 50 kDa (Millipore #UFC905024), or 100 kDa (Millipore #UFC910024) Amicon Ultra-15 centrifugal filters and standard protocols. Total protein concentrations were determined via BCA assay (Thermo Fisher Scientific #23225). SDS-PAGE was performed using either 8% gels for high molecular weight proteins (<100 kDa), or 12% gels for lower molecular weight proteins (<50 kDa). Proteins were transferred to PVDF membranes (Bio-Rad #1620174) in Towbin transfer buffer via overnight wet transfer at 30 V and 4 °C. Membranes were incubated at 4 °C overnight with the following primary antibodies: anti- β -actin mouse monoclonal antibody (1:5000; Sigma-Aldrich #A5316), anti-Calnexin rabbit polyclonal antibody (1:2000; Abcam #ab75801), anti-ERK5 rabbit polyclonal antibody (1:1000; Cell Signaling Technology #3372), anti-GAPDH mouse monoclonal antibody (1:1000; Santa Cruz Biotechnology #sc-32233), anti-HEG1 SKM9-2 mouse monoclonal antibody (5 μ g/mL; provided by collaborator), anti-KLF2 rabbit polyclonal antibody (1:1000; Sigma-Aldrich #09-820), anti-KLF4 rabbit monoclonal antibody (1:1000; Abcam #ab215036), anti-KRIT1 rabbit monoclonal antibody

Table 2.1 qPCR primer sequences

Primer	Species	Forward (5' → 3')	Reverse (5' → 3')
18S	Human/Mouse	AGGAATTGACGGAAGGGCACCA	GTGCAGCCCCGGACATCTAAG
CCM2	Human	CCTGCACAGCGATGACTC	ACCACCCACATCCACAGA
CCM2L	Human	CGTCCACACCTTCTTTCCAT	CGCAACGTGACCATGTAATC
CCM3	Human	GCCCCTCTATGCAGTCATGTA	AGCCTTGATGAAAGCGGCTC
eNOS	Human	GGCTGGTACATGAGCACTGA	TATCCAGGTCCATGCAGACA
eNOS	Mouse	CGCAAGAGGAAGGAGTCTAGCA	TCGAGCAAAGGCACAGAAGTGG
HEG1	Human	TCCTTTCCCGAGACACTTCC	AACACTGTCCGTTCAATGGC
HEG1	Mouse	GTCGGGTATCAGTTGGAGAAAAG	AGCTCTTGAGTGTTGGAATGG
KLF2	Human	CATCTGAAGGCGCATCTG	CGTGTGCTTTCGGTAGTGG
KLF2	Mouse	CTAAAGGCGCATCTGCGTA	TAGTGGCGGGTAAGCTCGT
KLF4	Human	ATCTCAAGGCACACCTGCG	CCTGGTCAGTTCATCTGAGCG
KLF4	Mouse	GCGAACTCACACAGGCGAGAAACC	TCGCTTCCTCTTCTCCGACACA
KRIT1	Human	GAAGCGCCTGTGAAGGAGATTC	ACAATATGCGAGTGGCCTCAAC

(1:1000; Abcam #ab196025), anti-MEKK3 mouse monoclonal antibody (1 μ g/mL; R&D Systems #MAB6095) and anti-VCAM-1 rabbit monoclonal antibody (1:1000; Abcam #134047) (178; 179). Membranes were incubated at room temperature for one hour with the following secondary antibodies: goat anti-mouse IgG HRP (Cayman Chemical #10004302) and goat anti-rabbit IgG HRP (Cayman Chemical #10004301). Protein bands were imaged using Immobilon Western chemiluminescent HRP substrate (Millipore #WBKLS0500) and the iBright FL1000 imaging system.

2.8 Immunocytochemistry

Cells were fixed using 4% PFA (Santa Cruz Biotechnology #sc-281692). 100 mm dish samples were cut to size for imaging using the Wondercutter S ultrasonic cutter (Micro-Mark #88195), while ibidi flow channel slides were used as provided. Cells were permeabilized with 0.1% Triton X-100 (Sigma Aldrich #X100) in PBS, blocked with 10% goat serum (Bio Ab Chem #72-0480) in PBST (Bio Basic #TB0560) and then incubated at 4 °C overnight with primary antibodies diluted in 5% goat serum in PBST. The following primary antibodies were used: anti-HEG1 10G10 mouse monoclonal antibody (25 μ g/mL; provided by collaborator), anti-VE-cadherin rabbit polyclonal antibody (1:1000; Abcam #ab33168), and anti-MEKK3 rabbit monoclonal antibody (1:500; Cell Signaling Technology #5727) (178; 179). Cells were next incubated with goat anti-mouse AlexaFluor 568 polyclonal (Thermo Fisher Scientific #A11004) and donkey anti-rabbit AlexaFluor 488 polyclonal (Thermo Fisher Scientific #A21206) secondary antibodies diluted in 1% BSA (Sigma Aldrich #A7906) PBST for 2 hours at room temperature. 100 mm dish samples were mounted with cover slips using Fluoroshield with DAPI (Sigma Aldrich #F6057), ibidi flow channel samples underwent Hoechst stain in PBS (Thermo Fisher Scientific #H3670). All images were taken at 63x magnification on a Zeiss LSM800 confocal microscope and analyzed with NIH ImageJ software.

2.9 siRNA knockdown

siRNA knockdown was performed using Oligofectamine transfection reagent (Invitrogen #12252-011) and standard protocol. Custom-made siRNA sequences are listed in **Table 2.2**. Additionally, siKLF2 (Thermo Fisher Scientific #1299001 siRNA ID HSS145585) and siKLF4 (Thermo Fisher Scientific #1299001 siRNA ID HSS113795) proprietary siRNAs were used.

2.10 Endothelial function studies

Monocyte adhesion to the endothelial monolayer surface was determined by exposing treated HAECs with fluorescently-labelled THP-1 monocytes (ATCC #TIB-202), as described previously (148; 180). Following exposure to siRNA and flow treatment, HAECs were washed in RPMI medium before adding 2',7'-bis(carboxyethyl)-5(6)-carboxyfluorescein-AM-labelled THP-1 monocytes (Thermo Fisher Scientific #B1150). After 30 minute incubation, unbound monocytes were washed away from the HAECs with PBS and HAEC-bound monocytes were fixed with 4% PFA (Santa Cruz Biotechnology #sc-281692). Bound monocytes were quantified by counting the number of fluorescent cells per high powered field using a fluorescent microscope.

Endothelial permeability was measured using FITC-avidin binding to cell biotinylated gelatin-coated culture substrate, as described previously (181). Briefly, HAECs were seeded on biotinylated gelatin-coated μ -Slide I^{0.4} Luer ibiTreat channels (ibidi #80176) for 24 hours, then treated with control or HEG1 siRNA for 24 hours, and then exposed to either static or ULS conditions using the ibidi pump system for 72 hours. Cells were then fixed, exposed to FITC-avidin, imaged using the BZ-X Series All-In-One fluorescence microscope (Keyence) and FITC fluorescent intensity was measured using NIH ImageJ software.

Endothelial tube formation was assessed using a Matrigel tube formation assay, as described previously (182). Following control or HEG1 siRNA knockdown and 24 hour exposure to static or

Table 2.2 siRNA sequences

siRNA	Forward (5' → 3')	Reverse (5' → 3')	Manufacturer
siCCM2	UAAAAAGAAGUUUACUGCAAUGUGA	UCACAUUGCAGUAAACUUCUUUUUAAG	IDT
siCCM2L	AUUUCACCAUGGAAUAUGAAGUCA	UUGACUUCAUAUCCAUGGUGAAAUGU	IDT
siCCM3	AGGTTTCTGCAGACAATCAAGGATA	UAUCCUUGAUUGUCUGCAGAAACCUCA	IDT
siHEG1	GCAGUGGAAUCGAGAAGAAACAGTA	UACUGUUUCUUCUCGAUCCACUGCAG	IDT
siKRIT1	CCAUCAGUUGUCAAAAGAUAAUACTA	UAGUAUUAUCUUUGACAACUGAUGGAA	IDT

ULS conditions using the cone and plate viscometer, HAECs were seeded in a growth factor reduced Matrigel (BD Bioscience) coated 96-well plate and incubated for 6 hours at 37 °C. Tubules were imaged and quantified by measuring total tubule length via NIH ImageJ software.

Endothelial migration was measured by scratch assay, as described previously (182; 183). HAEC monolayers treated with control or HEG1 siRNA and 24 hours of static or ULS conditions using the cone and plate viscometer were scratched with a 200 μ l pipette tip. Cells were washed once, and the 2% serum media was added in order to prevent confounding effects of FBS-induced cell proliferation. Images were taken at 0 – 24 hour timepoints and cell migration was determined by measuring the scratch area at each consecutive time point using NIH ImageJ software.

2.11 Plasmid overexpression and viral particle transduction

pCMV-GFP (Addgene #11153) and pCMV6-HEG1-MycDDK (Origene #RC212168) plasmid transfection in HAECs was performed using Lipofectamine 3000 transfection reagent (Invitrogen #L3000-015) and standard protocol. Ad-GFP (Welgen #V1020) and custom-made Ad-KLF4 (Welgen #S3000) viral particles were used to transduce HAECs using polybrene infection reagent (Santa Cruz Biotechnology #sc-134220) and standard protocol.

2.12 HEG1^{iECKO} mice

Heterozygous *loxP*-flanked (floxed) HEG1 C57Bl/6J mice (HEG1^{fl/+}) were purchased from Cyagen and genotyped using DNA gel electrophoresis. Homozygous floxed HEG1 mice (HEG1^{fl/fl}) were subsequently developed and crossed with tamoxifen-inducible, endothelial-specific Cdh5-CreERT2 mice provided by a collaborator to generate Cdh5-CreERT2^{+/-};HEG1^{fl/fl} mice, here called inducible, EC knockout HEG1 mice (HEG1^{iECKO}) (184). Genotype was confirmed by gel electrophoresis and endothelial-specific HEG1 knockout was confirmed after tamoxifen injection by

qPCR from endothelial-enriched thoracic aorta flushing samples, qHCR imaging of *en face* abdominal aorta samples, and scRNA-seq of thoracic aorta samples.

2.13 Mouse atherosclerosis studies

Carotid arteries were dissected at the time of sacrifice and photographed using a Moticom 2500 (Motic) attached to a EMZ-8TRD dissection microscope head (MEIJI Techno). Gross plaque burden was calculated by dividing the plaque-covered opaque area by the total area of the LCA using NIH ImageJ software, as described previously (180; 185). The LCA was subsequently fixed using 4% PFA (Santa Cruz Biotechnology #sc-281692), cut into two halves and then the two halves were sectioned longitudinally. Only sections taken from the center of artery were used for analysis. Oil red O (Sigma-Aldrich #MAK194) and Movat's pentachrome (StatLab #KTRMPPT) stainings were performed according to standard protocols. Stained longitudinal sections were imaged using the Nanozoomer-SQ Digital Slide Scanner microscope (Hamatsu #C13140-01). Intima-media thickness was calculated manually from pentachrome images in NIH ImageJ by dividing the intima and media area by artery length. Oil red O (ORO) lipid lesion area and pentachrome plaque content were determined using ilastik machine learning image analysis software (186). The software was trained to identify ORO positive pixels, and pixels corresponding to the appropriate colors in pentachrome stains. Identified pixels were then counted using NIH ImageJ and values were reported as number of positive pixels divided by artery length. CD68 immunostaining was performed using standard immunofluorescent staining protocols with anti-CD68 mouse monoclonal antibody (Bio-Rad #MCA1957), goat anti-rat AlexaFluor 568 polyclonal (Thermo Fisher Scientific #A11077), and Fluoroshield with DAPI (Sigma Aldrich #F6057). Mouse blood pressures were determined using the BP-2000 Blood Pressure Analysis system (Visitech Systems). Mice were trained for three consecutive days, and subsequent measurements were obtained by averaging 40 individual measurements of two

consecutive days, as per manufacturer recommended protocols. Serum cholesterol and triglyceride concentrations were determined using a Beckman CX7 biochemical analyzer at the Cardiovascular Specialty Laboratories, as reported previously (180).

2.14 Human coronary artery studies

Left anterior descending (LAD) coronary arteries were dissected from deidentified human hearts unsuited for transplantation donated to LifeLink of Georgia. Dissected LAD tissues were fixed in 4% PFA (Santa Cruz Biotechnology #sc-281692) overnight, paraffin-embedded, and then sectioned at a depth of 8 μ m. Prior to immunofluorescent staining, deparaffinization and antigen retrieval was performed, as described previously (187). Tissue sections were subsequently permeabilized with 0.1% Triton X-100 (Sigma Aldrich #X100) in PBS, blocked with 10% goat serum (Bio Ab Chem #72-0480) in PBST (Bio Basic #TB0560), incubated at 4 °C overnight with anti-HEG1 SKM9-2 mouse monoclonal antibody (25 μ g/mL; provided by collaborator), followed by Alexa Fluor-647 (Thermo Fisher Scientific, 1:500) secondary antibody for 2 hours at room temperature. Nuclei were counterstained using Fluoroshield with DAPI (Sigma Aldrich #F6057). All images were taken at 63x magnification on an LSM800 confocal microscope (Zeiss). HEG1 protein level was determined using background-corrected mean grey value analyzed with NIH ImageJ software. Plaque severity in whole artery sections and magnified areas of whole arteries were graded from I – VI by three independent graders using AHA histological classification guidelines (188). HEG1 staining in individual pictures was compared to plaque severity grade, as well as donor hypertension status. Deidentified donor information is displayed in **Table 2.3**.

Table 2.3 Human heart donor information

Data presented as category (units) [total number, sub-category number, or mean average].

n [30]	Age (year) [53.4]	Race [13B/16W/1H]	Sex [11F/19M]	BMI (kg/m ²) [32.5]	Hypertension [22Y/8N]	Diabetes [8Y/22N]	Smoking (Pack Years) [8.35]
1	61	Black	Female	Unknown	Yes	No	25
2	69	White	Female	Unknown	Yes	No	2.5
3	77	White	Male	Unknown	Yes	No	0
4	65	Black	Male	Unknown	Yes	Yes	0
5	63	White	Female	Unknown	No	No	0
6	61	Black	Male	Unknown	Yes	No	0
7	60	Black	Male	Unknown	No	Yes	0
8	45	Black	Female	Unknown	Yes	Yes	0
9	56	White	Male	Unknown	Yes	Yes	0
10	43	White	Male	Unknown	No	Yes	25
11	48	White	Female	34.1	Yes	No	51
12	38	White	Male	Unknown	No	No	12
13	45	Black	Female	Unknown	Yes	No	0
14	57	White	Male	38.2	Yes	No	12.5
15	69	White	Male	22.7	Yes	No	20
16	52	Black	Female	31.2	Yes	No	0
17	37	White	Male	35.3	No	No	0
18	48	White	Male	22.1	Yes	No	50
19	40	Hispanic	Male	33.9	No	No	0
20	49	White	Male	35.5	Yes	No	15
21	40	White	Male	27	No	No	0
22	47	Black	Male	36.3	Yes	Yes	30
23	40	Black	Female	26.3	Yes	Yes	0
24	56	White	Female	Unknown	Yes	Yes	7.5
25	72	Black	Female	Unknown	Yes	No	0
26	43	Black	Female	55.19	Yes	No	0
27	58	White	Male	Unknown	Yes	No	0
28	57	Black	Male	25.3	Yes	No	0
29	56	White	Male	Unknown	No	No	0
30	50	Black	Male	Unknown	Yes	No	0

2.15 Statistical analyses

All statistical analyses were performed using GraphPad Prism version 8.4.3 software. Specific replicate numbers are provided in the corresponding figure legends. N numbers represent biological replicates, and all data is presented using the mean average with error bars representing standard error of the mean (SEM). All datasets were analyzed for normality using the Shapiro-Wilk test, and for equal variance using the *F*-test for datasets with 2 groups, or the Brown-Forsythe test with groups of 3 or more. Comparisons between 2 groups were conducted using either two-tailed Student's *t*-test for parametric data, or two-tailed Mann-Whitney *U* test for non-parametric data. Comparisons between 3 or more groups were conducted using either one-way analysis of variance (ANOVA) or two-way ANOVA for parametric data, or Kruskal-Wallis *H* test for non-parametric data. Tukey's, Dunnett's, and Sidak's multiple comparison post-hoc tests were employed as appropriate following ANOVA. $P < 0.05$ was considered significant for all statistical tests that were performed.

3 Results

3.1 Aim 1 - Determine whether endothelial HEG1 expression is flow-sensitive.

3.1.1 Flow controls HEG1 expression and subcellular translocation in endothelial cells

We first identified HEG1 as a flow-sensitive gene by re-analyzing our prior scRNA-seq dataset of right (RCA) and left (LCA) carotid artery ECs from the mouse partial carotid ligation (PCL) study (15). In the study, LCAs were exposed to d-flow for 2 days or 2 weeks following the PCL, while the contralateral RCAs, exposed to s-flow in the same mice, were used as control. The violin plot analysis of the scRNA-seq result showed that HEG1 was primarily expressed in ECs and some in fibroblasts, but not in smooth muscle cells, macrophages, dendritic cells, and T cells (**Fig. 3.1a**). Interestingly, EC clusters found in s-flow conditions (E1-E4) expressed significantly higher levels of HEG1 compared to those ECs (E5-E8) exposed to d-flow, suggesting flow-sensitive regulation of HEG1 expression in ECs. The HEG1 result was further validated by re-analyzing an additional genome-wide gene array dataset (GSE182291) using the EC enriched bulk RNAs from the LCAs and RCAs obtained at three-time points: 1 day, 2 days, and 2 weeks following the PCL (**Fig. 3.1b**) (176). Moreover, we independently confirmed flow-dependent *Heg1* expression by qPCR in the EC-enriched samples from RCAs and LCAs obtained at 2 weeks post-PCL (**Fig. 3.1c**). The flow-dependent endothelial HEG1 expression in the mouse RCA and LCA was further demonstrated by using the hybridization chain reaction RNA fluorescence *in situ* hybridization (HCR) method for *HEG1* mRNA, with a concomitant CD31 antibody staining (**Fig. 3.1d**). These results clearly demonstrate that s-flow upregulates, while d-flow downregulates *Heg1* expression in ECs *in vivo* in mouse arteries.

To confirm these *in vivo* results and characterize HEG1 regulation by flow, human aortic endothelial cells (HAECs) were exposed to ULS (15 dyn/cm², mimicking s-flow), OSS (+5/-4

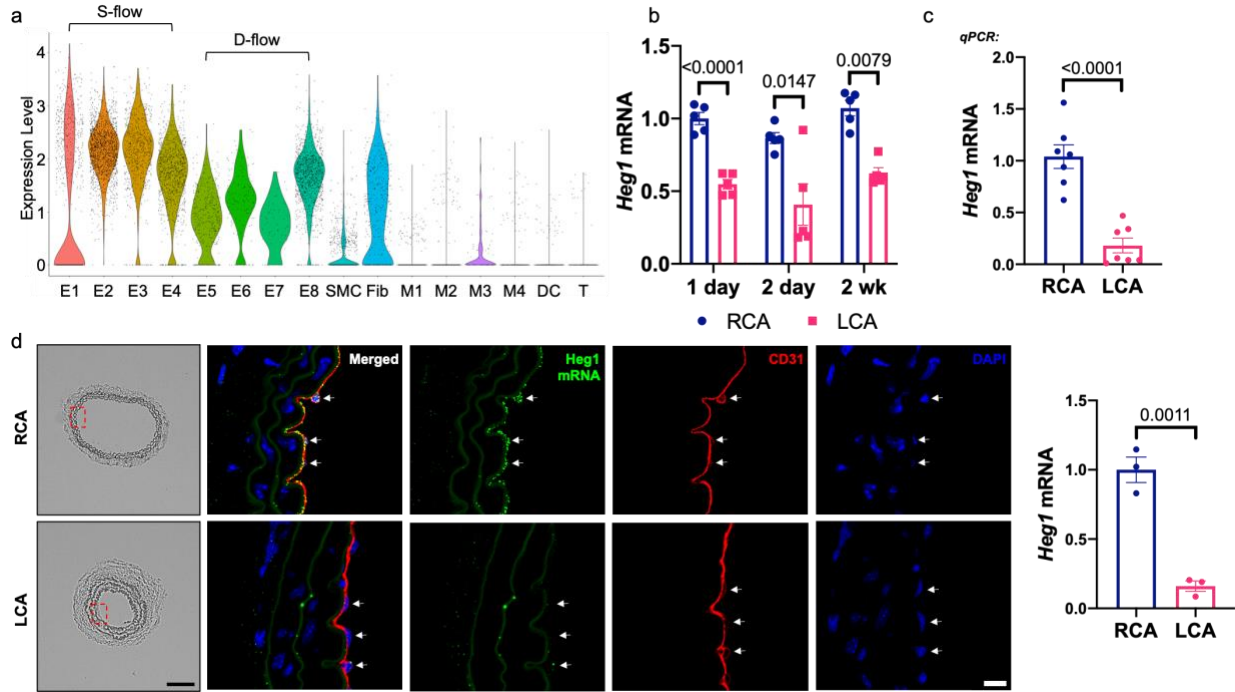


Figure 3.1 *Heg1* mRNA expression is regulated by flow *in vivo*.

(a) scRNA-seq analysis of right and left carotid arteries exposed to mouse PCL surgery demonstrate that HEG1 is expressed primarily in ECs (E1-8) and fibroblasts (Fib), and that EC expression of HEG1 is increased in s-flow exposed RCA ECs (E1-4) as compared to d-flow exposed LCA ECs (E5-8), as described previously (15). **(b-d)** Flow-sensitive *Heg1* mRNA expression was verified by **(b)** gene array at 1 day – 2 weeks post-PCL surgery, **(c)** qPCR at 2 weeks PCL, and **(d)** HCR RNA-FISH imaging at 2 weeks of PCL (scale bar left = 200 μ m; scale bar right = 10 μ m). Gene array, qPCR and HCR quantifications presented as fold change compared to control condition (bar on left).

dyn/cm² at 1 Hz, mimicking d-flow) using a cone-and-plate viscometer shear system. HAECs exposed to static conditions lacking flow were also used as a control. Exposure to ULS for 24 hours significantly increased HEG1 mRNA and protein expression as compared to the OSS and static conditions (**Fig. 3.2a, b**). Interestingly, HEG1 protein was also detected in the conditioned media (CM) from 24 hour ULS HAECs, but not the OSS or static media (**Fig. 3.2c**). To characterize this flow response further, we carried out 2 different time series studies. HEG1 protein in the cell lysate was initially reduced by ULS up to 3 hours, which rebounded after 12 hours under the s-flow condition (**Fig. 3.2d, e**). At the same time, HEG1 release into the media was detected as early as 30 minutes in response to ULS and continued to accumulate over time (**Fig. 3.2f, i**). The decrease in HEG1 protein in the cell lysate with a concomitant accumulation in the media during the first 3 hours was further confirmed by a shorter time course study (**Fig. 3.2g, i**). To address whether these protein expression changes were due to changes in mRNA levels, qPCR studies were conducted in the same cells. HEG1 mRNA level changes were detected only after 6 hours under ULS conditions (**Fig. 3.2e, h**). These results suggest that HEG1 protein is initially reduced during the first 3 hours due to its continuous release into the media without new transcription in response to ULS. After 6 hours, HEG1 mRNA and protein expression is recovered, indicating new transcription and translation in a flow-dependent manner.

To further characterize flow regulation of HEG1 protein in HAECs, HEG1 protein was examined by immunofluorescence microscopy. As expected, exposure to ULS for 24 hours increased HEG1 protein expression in HAECs compared to the static or OSS conditions (**Fig. 3.2j**). Surprisingly, unlike a diffuse staining pattern in static or OSS cells, HEG1 staining pattern showed a dramatic localization to the downstream side of endothelial cells in response to ULS. To further test whether flow regulates HEG1 location, HAECs were exposed to ULS in an acute study. As early as 2 minutes under ULS conditions, HEG1 protein was moving toward the downstream cell-cell junction

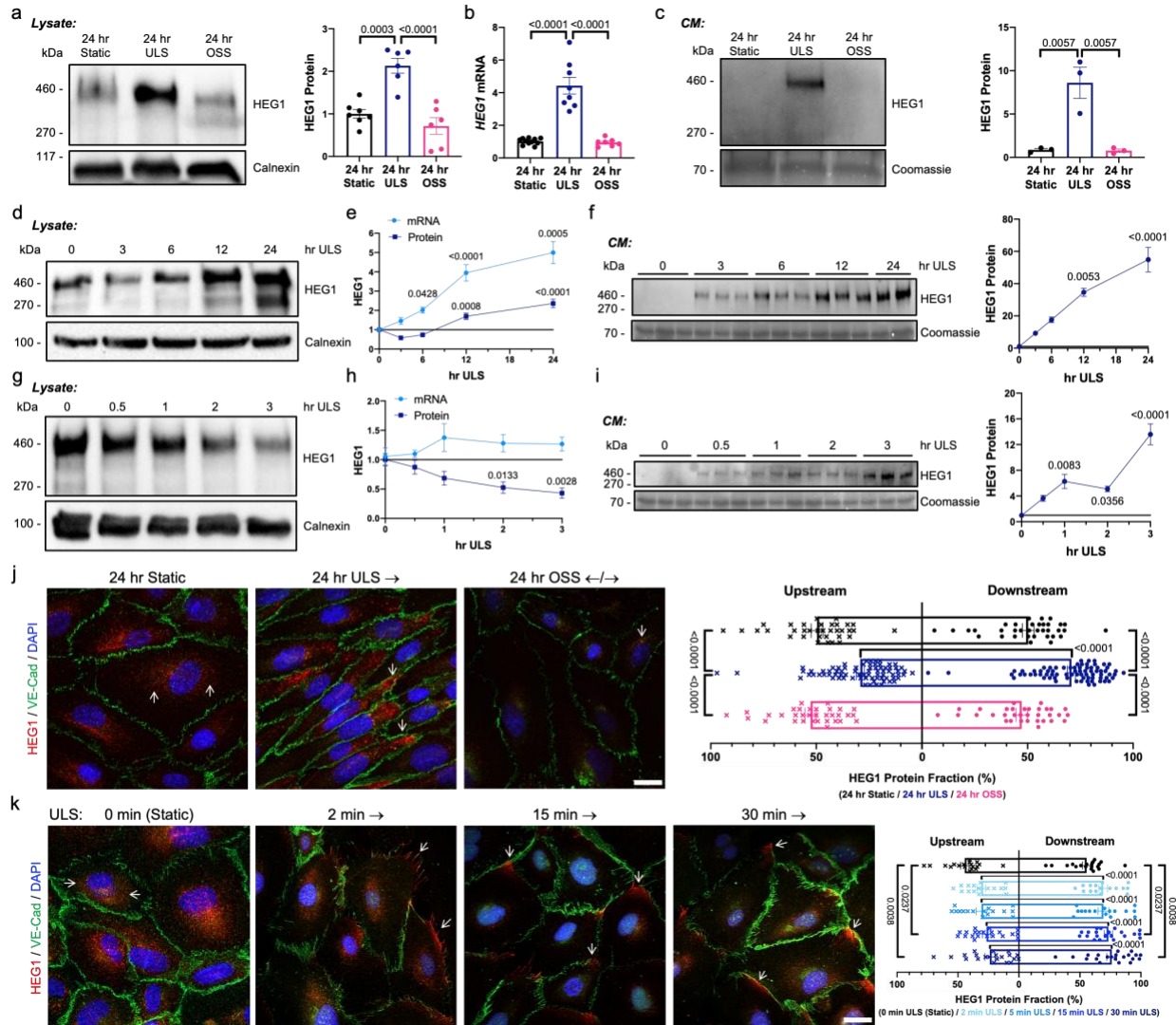


Figure 3.2 Flow controls HEG1 mRNA and protein expression, as well as protein subcellular localization *in vitro*

(a) HEG1 protein and (b) mRNA levels are elevated by 24 hr ULS as compared to 24 hr static and OSS. (c) HEG1 protein is detected in 24 hr ULS conditioned media (CM), but not in 24 hr static or OSS conditioned media. (d) 24 hr ULS time course shows that (e) HEG1 mRNA is elevated at 6 hr ULS and onward, and protein at 12 hr ULS and onward ($n = 3-7$). (f) HEG1 protein in conditioned media is present at 3 hr ULS and increases linearly with time ($n = 3-5$). (g) 3 hr ULS time course shows that (h) HEG1 mRNA does not change, but protein decreases at 2 – 3 hr ULS ($n = 6$). (i) HEG1 protein is observed in conditioned media as soon as 0.5 hr ULS and increases linearly with time ($n=3$). (j) HEG1 protein is centrally located on the apical surface of endothelial cells in 24 hr static and OSS conditions, but migrates to the downstream pole of elongated endothelial cells in 24 hr ULS (scale bar = 10 μm). (k) 30 minute ULS time course shows that HEG1 migration to downstream pole of EC begins within minutes of ULS exposure (scale bar = 10 μm). Quantifications in (a-i) presented as fold change compared to control condition on left.

area as marked by the VE-cadherin staining (**Fig. 3.2k**). These results demonstrate that s-flow rapidly induces HEG1 protein translocation to the downstream side of ECs.

Taken together, these *in vitro* and *in vivo* results demonstrate that flow regulates HEG1 gene and protein expression, and polarized localization and secretion of HEG1 protein.

3.1.2 Flow-induced HEG1 transcription is promoted by increased chromatin availability and performed by transcription factors KLF2 and KLF4

To understand how HEG1 is transcribed in response to stable flow, single cell assay for transposase-accessible chromatin using sequencing (scATAC-seq) data from RCA and LCA ECs of mice exposed to PCL surgery for either two days or two weeks, mirroring the scRNA-seq studies, were first assessed (15). scATAC-seq analysis showed that the chromatin accessibility at the transcription start site (TSS) and putative promoter region (1500 bp region upstream of TSS) was greater in the s-flow exposed RCA E1-4 clusters as compared to that of the d-flow exposed LCA E5-8 clusters (**Fig. 3.3a**). This result indicates that HEG1 transcription in ULS is in part controlled by epigenetic regulation of HEG1 promoter region chromatin accessibility.

Based on previous literature indicating that *klf2a* transcribes *heg1* in zebrafish, and the fact that the majority of ULS-induced endothelial genes in humans are transcribed by KLF2 and KLF4, potential KLF2 and KLF4 binding sites in the putative promoter region of HEG1 were assessed (189; 190). 7 KLF4 binding motifs were identified in the human HEG1 promoter region and 10 in the mouse promoter region using the JASPAR CORE online database (**Fig. 3.3b**). With this information, targeted studies examining KLF2 and KLF4 control of HEG1 transcription in ULS were performed.

Using the cone-and-plate viscometer shear system on HAECs, 24 hr ULS plus KLF4 siRNA knockdown blocked ULS-induced upregulation of HEG1 expression as compared to 24 hr ULS plus

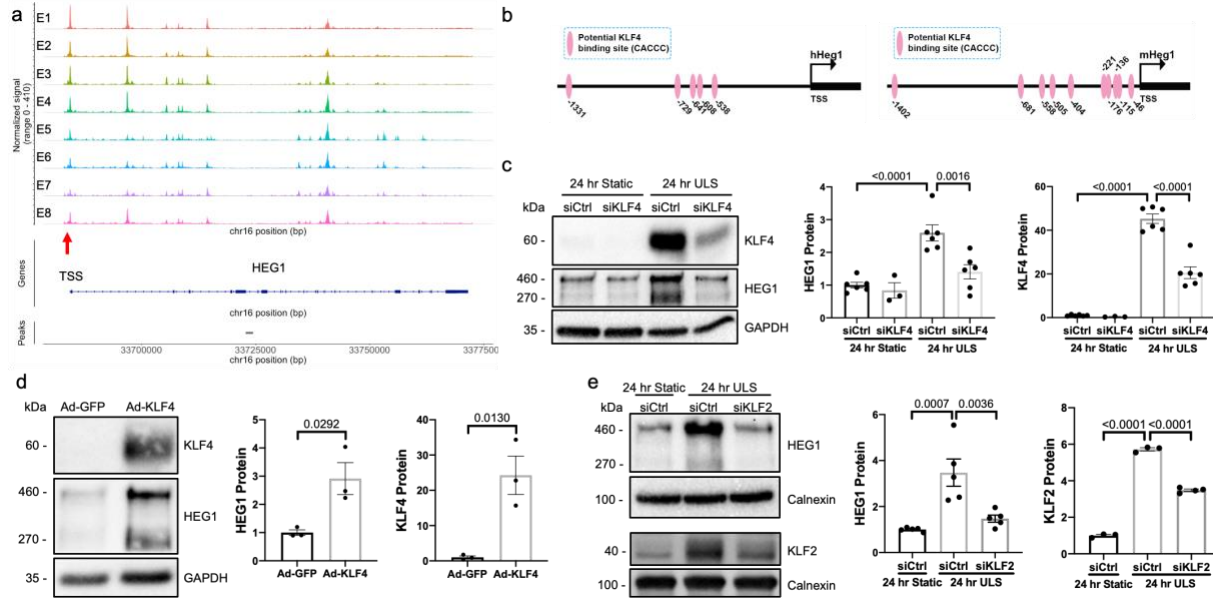


Figure 3.3 Increased chromatin availability and the transcription factors KLF2 and KLF4 control flow-induced HEG1 expression

(a) scATAC-seq analysis of right and left carotid arteries exposed to mouse PCL surgery demonstrate that the HEG1 promoter region (red arrow) has increased availability in s-flow exposed RCA ECs (E1-4) as compared to d-flow exposed LCA ECs (E5-8), as described previously (15). (b) The HEG1 promoter region has multiple KLF4 binding sites, as predicted by JASPAR CORE. (c) 24 hr ULS plus siKLF4 blocks ULS-induced HEG1 protein expression. (d) Plasmid overexpression of KLF4 induces HEG1 protein expression. (e) 24 hr ULS plus siKLF2 blocks ULS-induced HEG1 expression. Quantifications presented as fold change compared to control condition on left.

siRNA control (**Fig. 3.3c**). To prove that KLF4 expression is sufficient for HEG1 upregulation, HAECs were infected with either adenovirus GFP control (Ad-GFP) or adenovirus KLF4 (Ad-KLF4), and HEG1 protein levels were assessed. Ad-KLF4 significantly increased HEG1 expression as compared to Ad-GFP control (**Fig. 3.3d**). Additionally, 24 hr ULS plus KLF2 siRNA knockdown blocked ULS-induced upregulation of HEG1 expression as compared to 24 hr ULS plus siRNA control (**Fig. 3.3e**). These results indicate that KLF2 and KLF4 are both necessary for HEG1 expression upregulation in ULS. Together, these data indicate that ULS induces HEG1 transcription via epigenetically increasing HEG1 promoter region chromatin accessibility and via the activity of the ULS-induced transcription factors KLF2 and KLF4.

3.2 Aim 2 - Determine the role of HEG1 in endothelial function and dysfunction.

3.2.1 HEG1 mediates multiple ULS-induced functional changes in HAECs

Having established that HEG1 is a flow-sensitive gene and protein increased by s-flow, we next tested its functional significance by siRNA knockdown of HEG1 in HAECs under flow conditions. As expected, ULS inhibited monocyte adhesion, permeability, tube formation, and migration responses of HAECs, which were prevented by HEG1 knockdown using siRNA (**Fig. 3.4a, b, c, d**). In addition, HEG1 knockdown by the siRNA also prevented the ULS-mediated effects on VCAM1 suppression and eNOS induction in HAECs (**Fig. 3.4e, f**). These results demonstrate that HEG1 plays a critical role in mediating the s-flow-induced regulation of endothelial function.

3.2.2 HEG1 mediates flow-induced KLF2/4 expression by the MEKK3-MEK5-ERK5-MEF2 pathway

We next studied the mechanisms by which HEG1 mediates the s-flow effects in ECs. Given the significant and wide-ranging effects of HEG1 knockdown in ULS conditions, including anti-

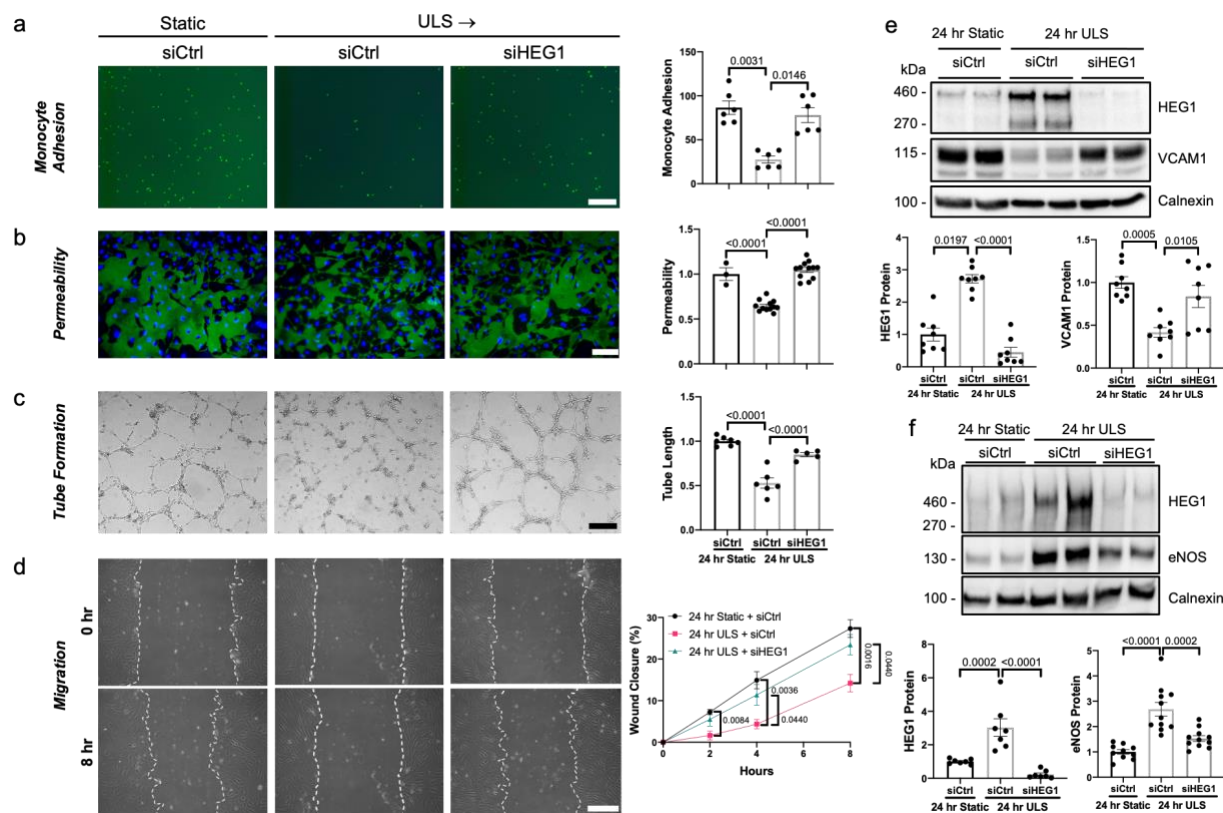


Figure 3.4 HEG1 mediates multiple ULS-induced functional changes in HAECs

HEG1 knockdown prior to 24 hr ULS prevents reduction in **(a)** endothelial monocyte adhesion (scale bar = 200 μm), **(b)** endothelial permeability (scale bar = 100 μm), **(c)** endothelial tube formation (scale bar = 200 μm), and **(d)** endothelial migration (scale bar = 200 μm). **(e)** Inhibitory effect of ULS on VCAM1 protein expression is reversed by HEG1 knockdown. **(f)** HEG1 knockdown reduces ULS-induced eNOS protein expression. Monocyte adhesion quantified as monocytes per field. Migration quantified as percent reduction in scratch wound area as compared to 0 hr. All other quantifications presented as fold change compared to control condition on left.

inflammatory effects and eNOS expression, we hypothesized that HEG1 regulates KLF2/4 expression, which in turn mediate the s-flow effects. To test the hypothesis, KLF2/4 mRNA and protein expression was examined in HAECs treated with siHEG1 and ULS at 3 hour. We chose this relatively early time point to examine the intermediate signaling pathways regulating KLF2/4 expression, when HEG1 expression level is reduced, as shown above (**Fig. 3.2d, g**). As expected, ULS significantly induced KLF2/4 mRNA and protein expression, which was blunted by HEG1 knockdown by siRNA (**Fig. 3.5a-c**). These results clearly demonstrate the critical role of HEG1 in regulating KLF2/4 expression by ULS.

ULS regulates KLF2/4 expression by activating the MEKK3-MEK5-ERK5-MEF2 pathway in ECs (124; 191; 192). We tested whether HEG1 regulation of KLF2/4 expression by ULS was mediated by the MEKK3-MEK5-ERK5-MEF2 pathway by using the well-known, specific pharmacological inhibitors and HEG1 siRNA knockdown. As expected, ULS increased ERK5 phosphorylation, which was prevented by HEG1 siRNA knockdown, providing crucial evidence that HEG1 regulates ERK5, the key signaling protein in the ULS-mediated KLF2/4 expression pathway (**Fig. 3.5a, b**). Next we treated HAECs with specific inhibitors of MEKK3 (Ponatinib), MEK5 (BIX02189), and ERK5 (XMD8-92) to test the hierarchical relationship between HEG1 and the MEKK3-MEK5-ERK5-KLF2/4 pathway in response to ULS. Treatment with Ponatinib inhibited ULS-induced ERK5 phosphorylation and KLF2/4 expression, but had no effect on HEG1 expression under ULS conditions (**Fig. 3.5d, e, f**). Similarly, the inhibitors of MEK5 and ERK5 blocked the ULS-induced ERK5 phosphorylation and KLF2/4 expression without affecting HEG1 protein levels under ULS conditions (**Fig. 3.6a-f**). These results demonstrate that HEG1 is an upstream regulator of the ULS-induced MEKK3-MEK5-ERK5-KLF2/4 pathway in ECs.

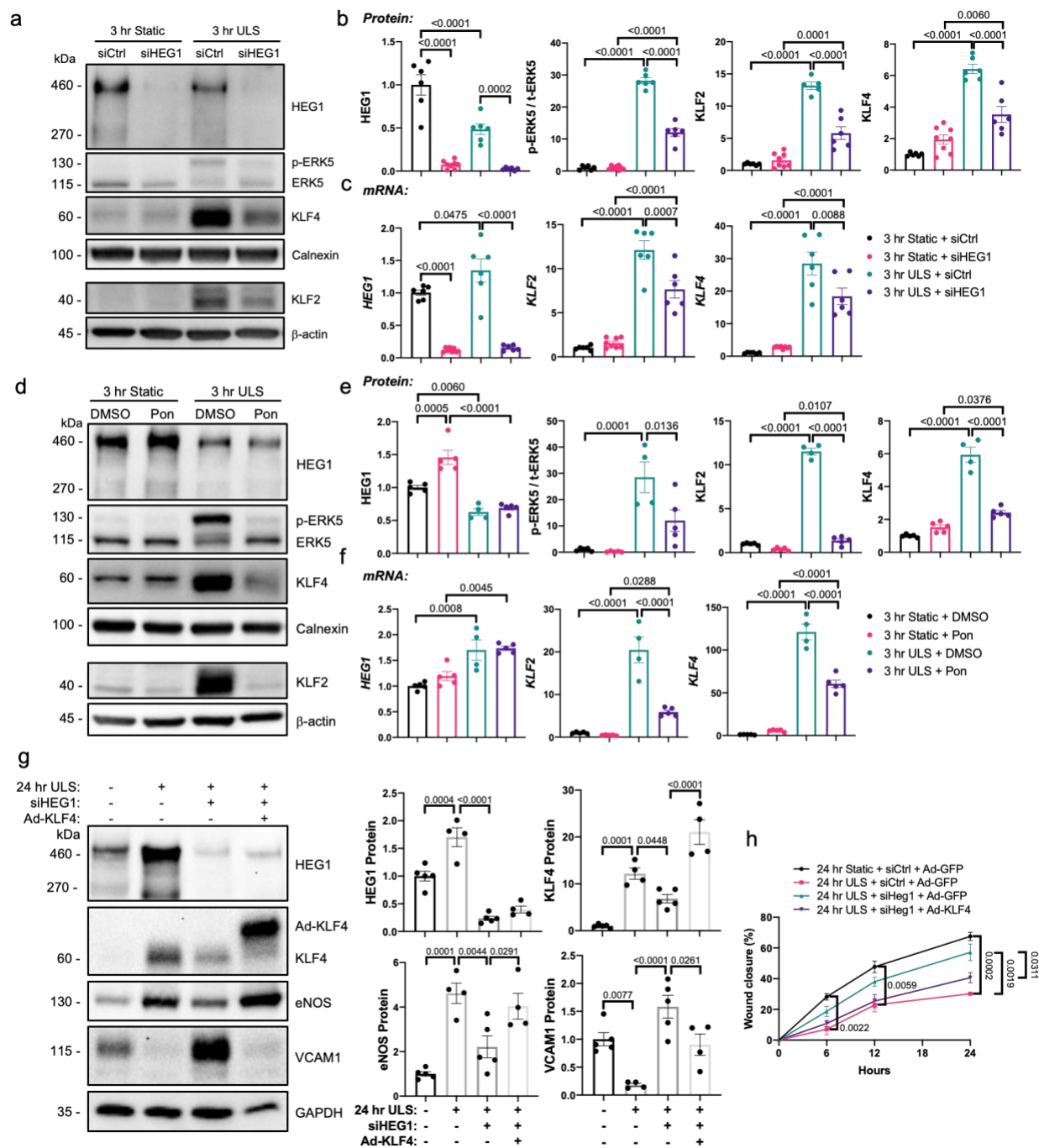


Figure 3.5 HEG1 mediates ULS-induced KLF2/4 expression in HAECs via MEKK3-MEK5-ERK5-MEF2 pathway

(a-c) HEG1 siRNA knockdown reduces ERK5 phosphorylation, and KLF2/4 mRNA and protein expression at 3 hr ULS. (d-f) Ponatinib (Pon) inhibition of MEKK3 prior to 3 hr ULS prevents ERK5 phosphorylation, and KLF2/4 mRNA and protein expression. (g) HEG1 siRNA knockdown plus KLF4 overexpression prior to 24 hr ULS reverses effects of HEG1 knockdown on VCAM1 and eNOS protein expression. (h) HEG1 siRNA knockdown plus KLF4 overexpression prior to 24 hr ULS reverses pro-migratory effect of HEG1 knockdown on ULS-exposed HAECs. Migration

quantified as percent reduction in scratch wound area as compared to 0 hr. All other quantifications presented as fold change as compared to control condition on left.

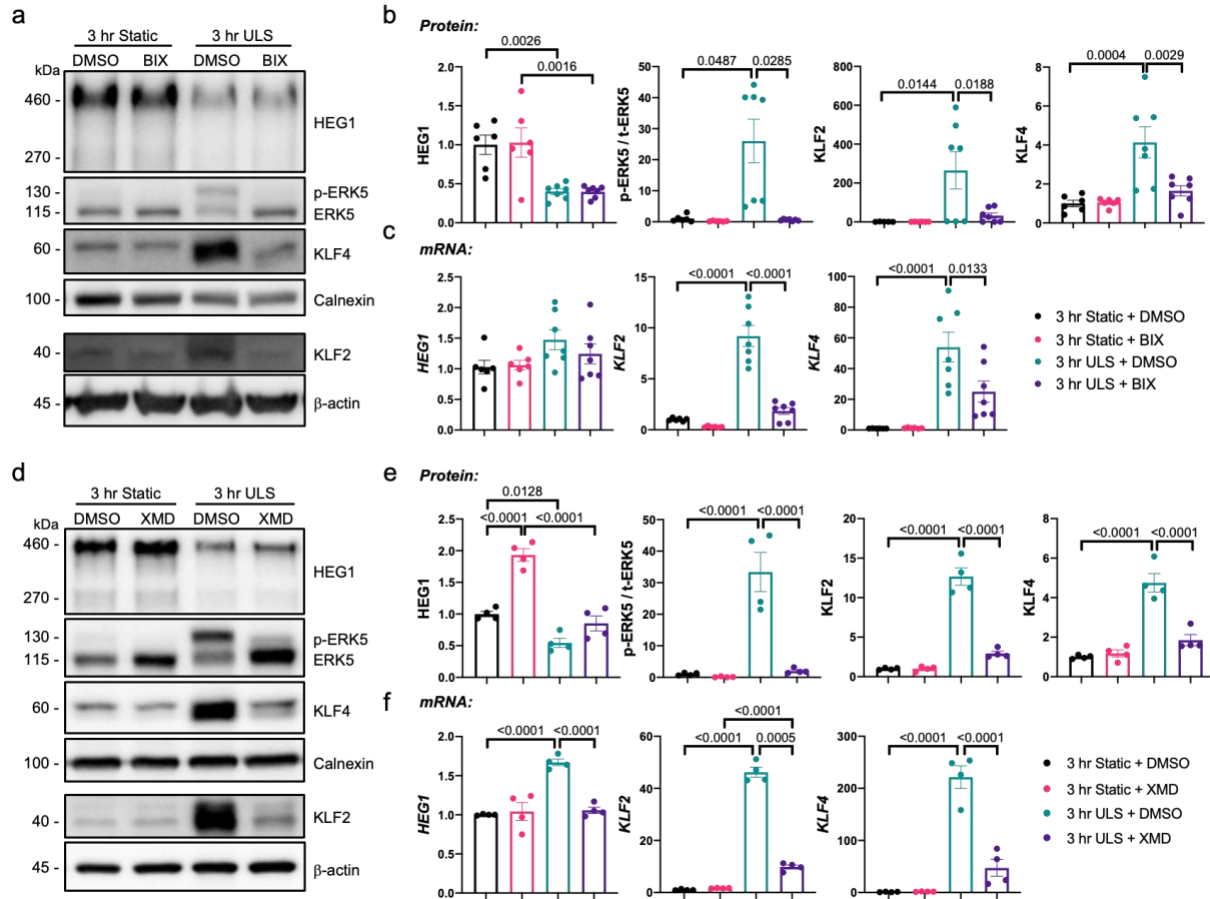


Figure 3.6 MEK5 and ERK5 inhibition blocks ULS-induced KLF2/4 expression

(a-c) MEK5 inhibition using BIX-02189 (BIX) blocks ERK5 phosphorylation, and KLF2/4 mRNA and protein expression in 3 hr ULS, but does not effect HEG1 protein loss. **(d-f)** ERK5 inhibition using XMD8-92 blocks ERK5 phosphorylation, and KLF2/4 mRNA and protein expression in 3 hr ULS, but does not effect HEG1 protein loss. Quantifications presented as fold change compared to control on left.

Finally, to confirm that HEG1 regulation of KLF2 and KLF4 control the functional changes observed when HEG1 is knocked down in ULS conditions, KLF4 replacement in 24 hr ULS plus siHEG1 treated HAECs was performed. Ad-KLF4 reversed the effects of HEG1 knockdown on eNOS and VCAM1 protein expression, as well as EC migration, indicating that at least some of the functional changes controlled by HEG1 are mediated by KLF4 (**Fig. 3.5g, h**).

3.2.3 HEG1 controls protein level of MEKK3-inhibitor KRIT1 by co-secretion in response to flow

We next studied how HEG1 regulates the MEKK3-MEK5-ERK5-KLF2/4 pathway. HEG1 is known to bind krev interaction trapped protein 1 (KRIT1) and ras interacting protein 1 (RASIP1) (166; 193). KRIT1, also known as cerebral cavernous malformation 1 (CCM1) serves as an inhibitor of MEKK3 activation (194-196). The dissociation of KRIT1 and the CCM complex from MEKK3 is known to activate the MEKK3 pathway and downstream KLF2/4 expression (197; 198). Therefore, we tested whether HEG1 activates the MEKK3-MEK5-ERK5-KLF2/4 pathway in a KRIT1-dependent manner. siRNA knockdown of KRIT1 enhanced ERK5 phosphorylation and KLF2/4 expression in response to ULS, confirming the repressive role of KRIT1 in activation of the MEKK3-MEK5-ERK5-KLF2/4 pathway (**Fig. 3.7a**). CCM complex members CCM2, CCM2-like (CCM2L) and CCM3 negatively regulated this pathway activation, as well (**Fig. 3.8a-f**). We next tested whether flow regulates KRIT1 expression. Interestingly, ULS reduced KRIT1 protein levels in the cell lysate, despite the fact that KRIT1 mRNA expression was increased by ULS (**Fig. 3.7b**). Since KRIT1 is known to bind HEG1, and HEG1 protein is released into the media in response to ULS, we tested whether KRIT1 protein was also secreted into the media with HEG1. Surprisingly, we found that KRIT1 was released into the media in response to ULS, but not

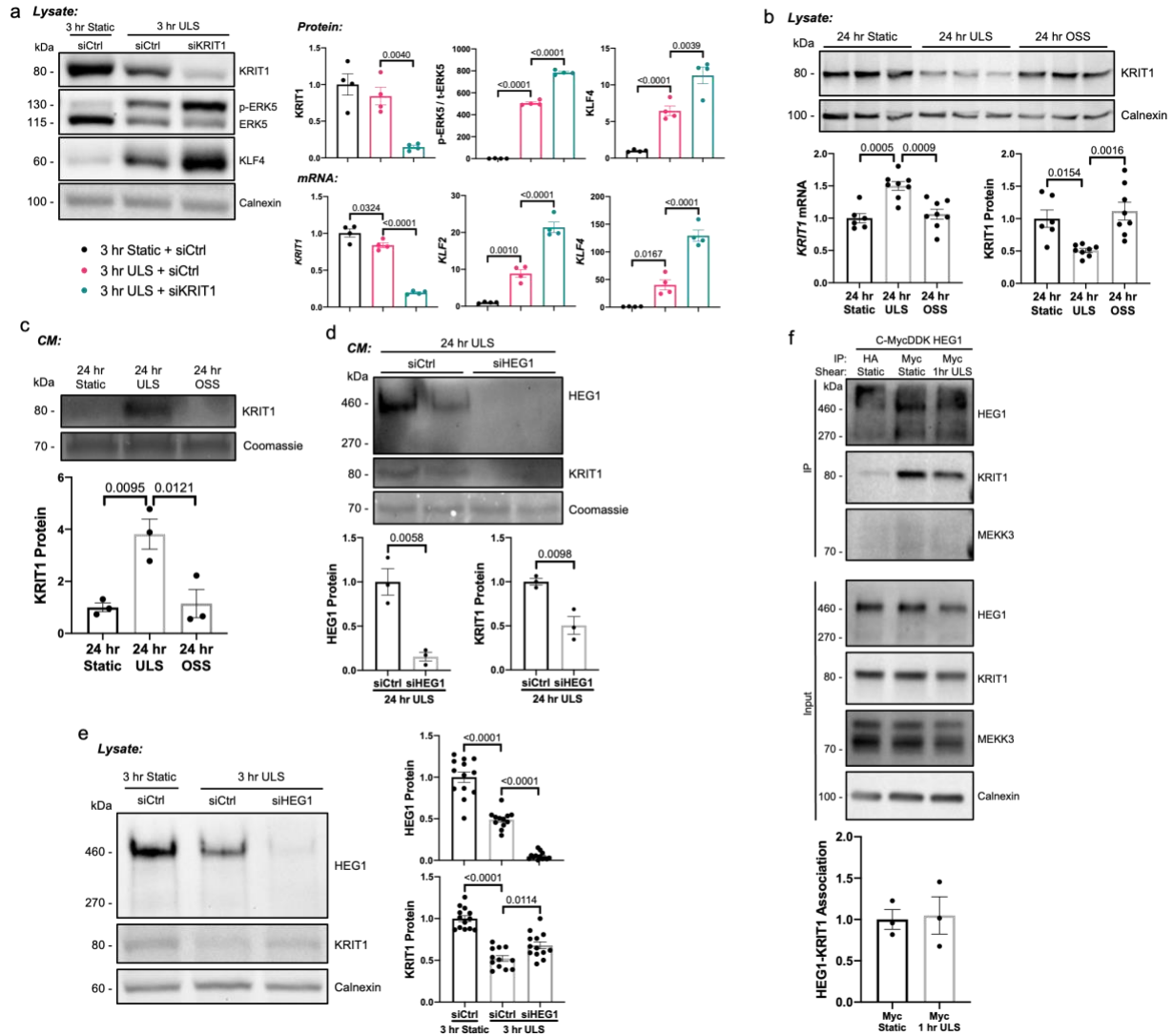


Figure 3.7 KRIT1 inhibits MEKK3-MEK5-ERK5-MEF2 pathway, and HEG1 mediates ULS-induced secretion of KRIT1

(a) KRIT1 siRNA knockdown increases ERK5 phosphorylation, and KLF2/4 mRNA and protein expression 24 hr ULS. (b) KRIT1 protein expression is decreased in 24 hr ULS, while mRNA expression is slightly elevated. (c) KRIT1 protein is found in conditioned media (CM) from 24 hr ULS samples, but not 24 hr static or OSS media. (d) HEG1 siRNA knockdown blocks ULS-induced KRIT1 secretion into the conditioned media. (e) HEG1 knockdown prior to 3 hr ULS increases intracellular levels of KRIT1. (f) HEG1 and KRIT1 remain bound to each other in both static and ULS conditions. MEKK3 is not pulled down along with HEG1 and KRIT1. Quantifications presented as fold change as compared to control conditions on left.

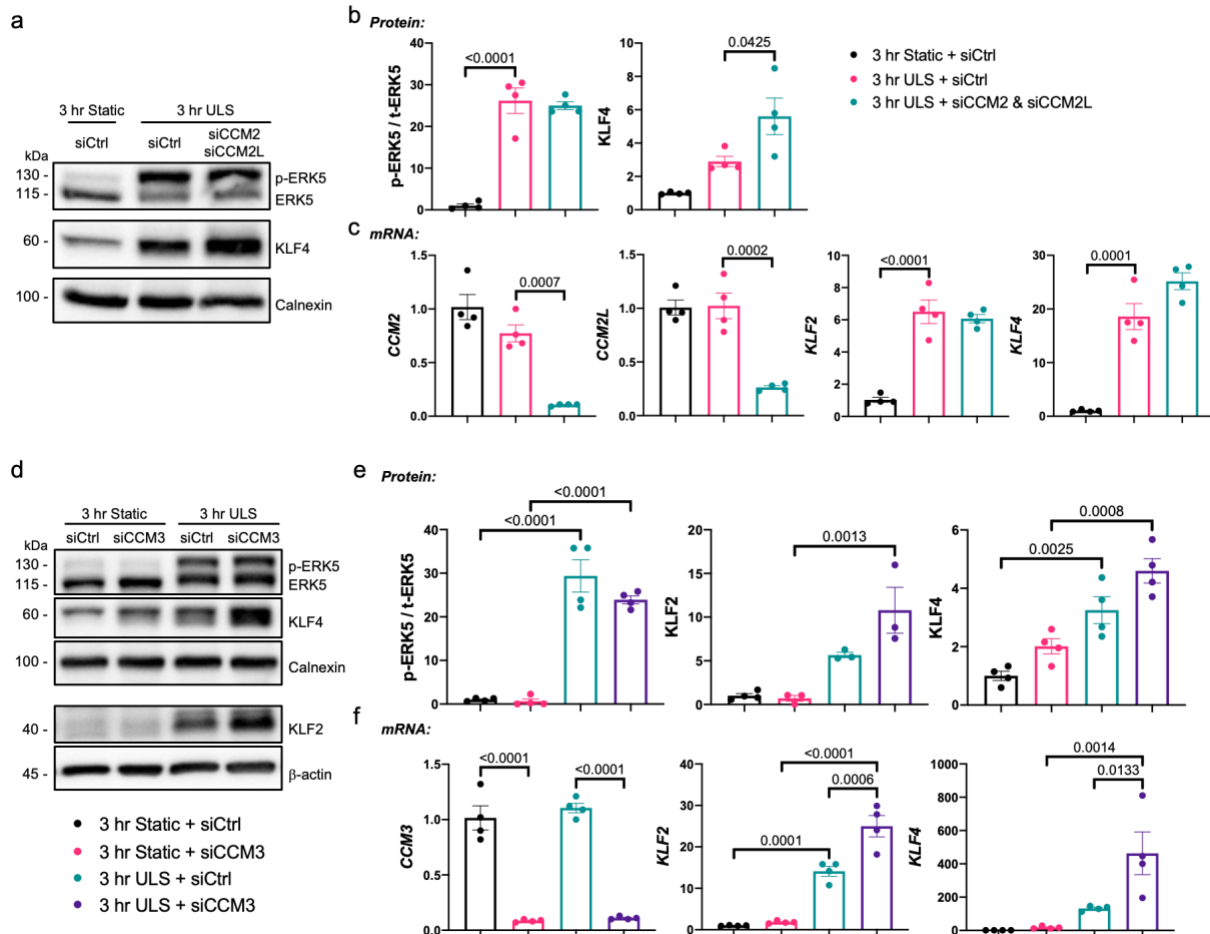


Figure 3.8 CCM2/2L and CCM3 inhibit KLF2/4 induction in ULS

(a-c) Simultaneous CCM2 and CCM2L siRNA knockdown increase KLF4 protein expression at 24 hr ULS. **(d-f)** CCM3 siRNA knockdown increases KLF2 and KLF4 mRNA expression at 3 hr ULS. Quantifications presented as fold change compared to control on left.

static or OSS conditions (**Fig 3.7c**). Knockdown of HEG1 prevented KRIT1 release into the media under the ULS condition (**Fig. 3.7d**), while the KRIT1 protein in the cell lysate was restored toward the control (**Fig. 3.7e**). These results demonstrate that KRIT1 is released into the media in a HEG1-dependent manner. This result was further supported by co-immunoprecipitation of HEG1 with KRIT1, which remained the same regardless of shear conditions (**Fig. 3.7f**). In this study, we did not observe MEKK3 in the co-immunoprecipitates. Together, these results raise an interesting hypothesis that ULS pulls HEG1 out of endothelial cells along with the MEKK3-inhibitor KRIT1, thereby activating the MEKK3-MEK5-ERK5-KLF2/4 pathway.

3.3 Aim 3 - Determine the role of HEG1 in the pathogenesis of atherosclerosis.

3.3.1 HEG1^{iECKO} mice have reduced endothelial KLF2/4 and eNOS expression and increased levels of atherosclerosis

Having found that HEG1 mediates several ULS-induced, atheroprotective functional changes in ECs via control of KLF2 and KLF4 induction *in vitro*, the atheroprotective effects of HEG1 were next assessed *in vivo*. To perform these studies, inducible endothelial cell-specific HEG1 knockout mice (HEG1^{iECKO}) were developed by cross-breeding EC-specific inducible Cre mice (Cdh5-CreERT2;HEG1^{WT}) with homozygous loxP-flanked HEG1 mice (HEG1^{fl/fl}). For the atherosclerosis studies, HEG1^{iECKO} mice were compared to Cdh5-CreERT2;HEG1^{WT} (HEG1^{WT}) mice. Studies were conducted over six week periods, as follows: all mice were first injected with tamoxifen for five consecutive days in the first week to induce HEG1 knockout. Mice were then allowed to rest and accommodate to their genetic changes for two weeks. At week three, all mice were injected with AAV-PCSK9 and fed high-fat diet in order to induce hypercholesterolemia (31). At week four, PCL surgery was performed on all mice and atherosclerosis was allowed to develop for two weeks after the surgery (**Fig. 3.9a**). At week six, the mice were sacrificed. Plasma was collected to measure lipid and

cholesterol concentrations, and livers were isolated to verify AAV-PCSK9 function via LDL receptor (LDLR) western blot. Thoracic aorta ECs were flushed with Qiazol to verify HEG1 knockout via qPCR, as previously described (32). Abdominal aorta samples were retained for confirmatory qHCR imaging. Right and left carotid arteries were isolated for gross plaque imaging, and longitudinal sectioning. Longitudinal LCA sections were subsequently stained with Movat's pentachrome and Oil red O stain. Immunofluorescent imaging of monocyte marker CD68 was also performed. Mice were excluded if they did not have total plasma cholesterol concentrations above 300 mg/dL or did not have visible plaque on gross imaging.

A total of 22 HEG1^{WT} (8 male, 14 female) and 27 HEG1^{iECKO} mice (9 male, 18 female) from seven separate experiments were included in this analysis. Both groups of mice had equivalent ages (~12 weeks), and weights (~20 g) at the time of sacrifice (**Fig. 3.10a-c**). qPCR analysis of *Heg1* mRNA from thoracic aorta ECs of the HEG1^{iECKO} mice demonstrated clear knockout, which was confirmed by *en face* HCR imaging of the abdominal aorta (**Fig. 3.9b, c**). Importantly, HEG1^{iECKO} mice were found to have significantly reduced levels of *Klf2*, *Klf4* and their target gene, *enos* in the thoracic aorta ECs, confirming the *in vitro* results demonstrating the necessity of HEG1 expression for the induction of KLF2 and KLF4.

Gross imaging of the excised mouse carotids demonstrated that atherosclerotic plaques developed in the d-flow exposed LCAs and that the HEG1^{iECKO} LCA plaques were increased in size as compared to the HEG1^{WT} mice (**Fig. 3.9d**). Microscopic analysis of longitudinal LCA sections stained with Oil Red O and Movat's pentachrome stains show that the HEG1^{iECKO} mice had increased lipid deposition, increased intima-media thickness, and advanced plaque features such as increased necrotic core area and increased fibronoid/muscle content, as compared to HEG1^{WT} mice (**Fig. 3.9e-j**). Furthermore, immunofluorescent CD68 staining demonstrated that the HEG1^{iECKO} mice have increased monocyte infiltration (**Fig. 3.9k**). Differences in atherosclerotic plaque size and maturity

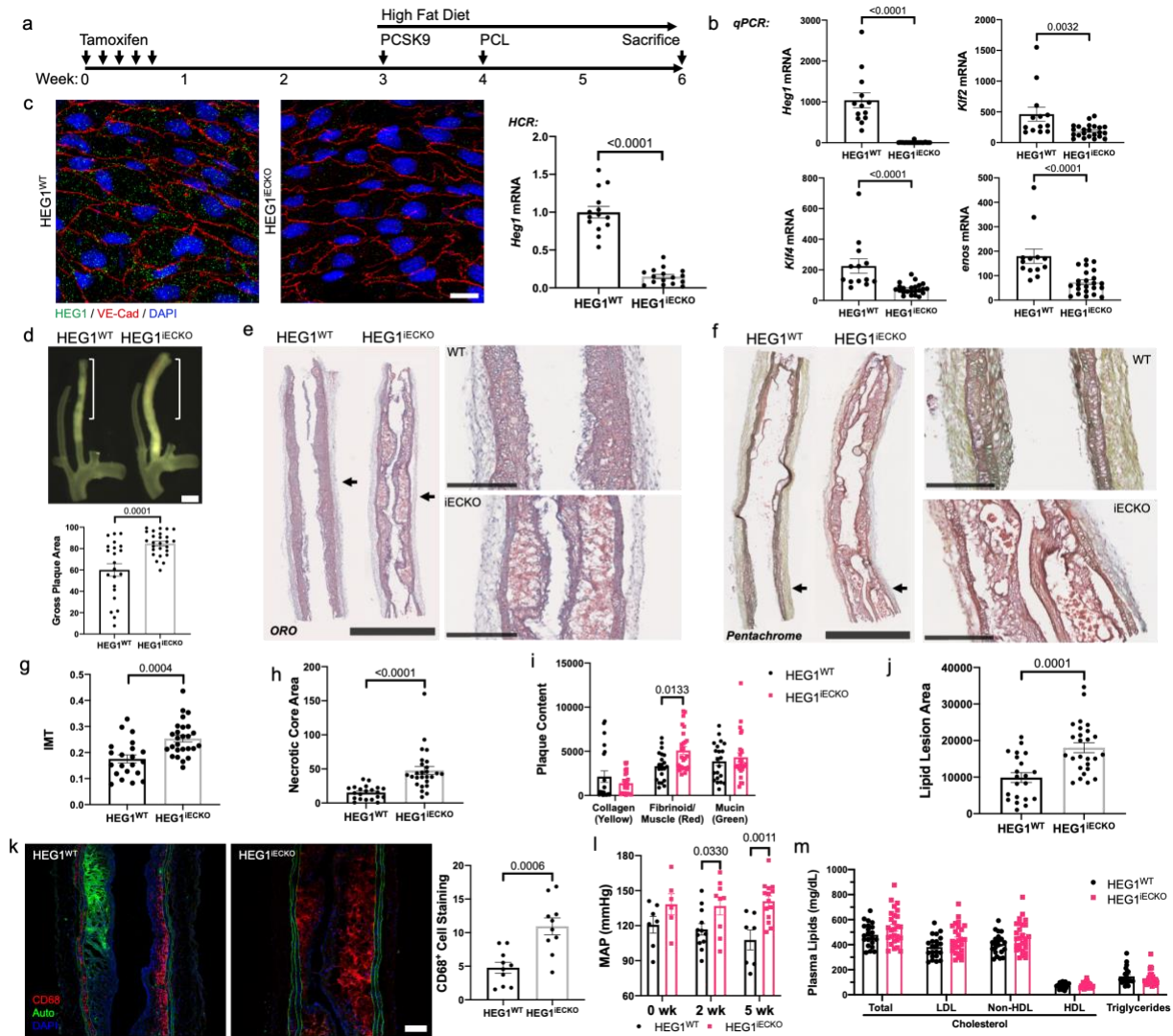


Figure 3.9 EC-specific HEG1 knockout reduces endothelial KLF2/4 expression and increases atherosclerosis in mice exposed to 2 week PCL

(a) 6-week timeline of HEG1 knockout plus PCL experiment. (b) qPCR analysis of thoracic aorta ECs shows *Heg1* knockout and significant decreases in *Klf2*, *Klf4* and *enos* mRNA expression. (c) HCR RNA-FISH imaging of *en face* abdominal aorta ECs demonstrate clear decrease in *Heg1* mRNA in HEG1^{IECKO} mice (scale bar = 10 μ m). (d) Gross image analysis of left carotid arteries shows increased opaque plaque area in HEG1^{IECKO} mice (scale bar = 1 mm). (e) Oil red O (ORO) staining of longitudinal LCA sections demonstrates (j) increased lipid deposition and (h) increased necrotic core area in arterial walls of HEG1^{IECKO} mice (scale bars = 1 mm, 500 μ m). (f) Pentachrome staining of LCA sections demonstrates (g) increased intima-media thickness (IMT) and (i) fibrinoid/muscle tissue staining in HEG1^{IECKO} mice (scale bars = 1 mm, 500 μ m). (k) HEG1^{IECKO} mice have increased CD68 positive leukocyte infiltration into LCA wall (scale bar = 100 μ m). (l) HEG1^{IECKO} mice have elevated mean arterial pressures (MAP) as compared to HEG1^{WT} controls. (i) HEG1^{WT} and HEG1^{IECKO} mice had equivalent plasma concentrations of total, LDL, non-HDL and HDL cholesterol, as well as triglycerides. qPCR quantifications presented as transcripts per million *18S*

control (TPM). HCR quantification presented as fold change as compared to control on left. Gross plaque area quantified as percent plaque area over LCA area. IMT and necrotic core area were calculated as pixel area divided by artery length. Plaque content and lipid lesion area were calculated as number of color positive pixels divided by artery length. CD68 staining is presented as average red fluorescence intensity per field.

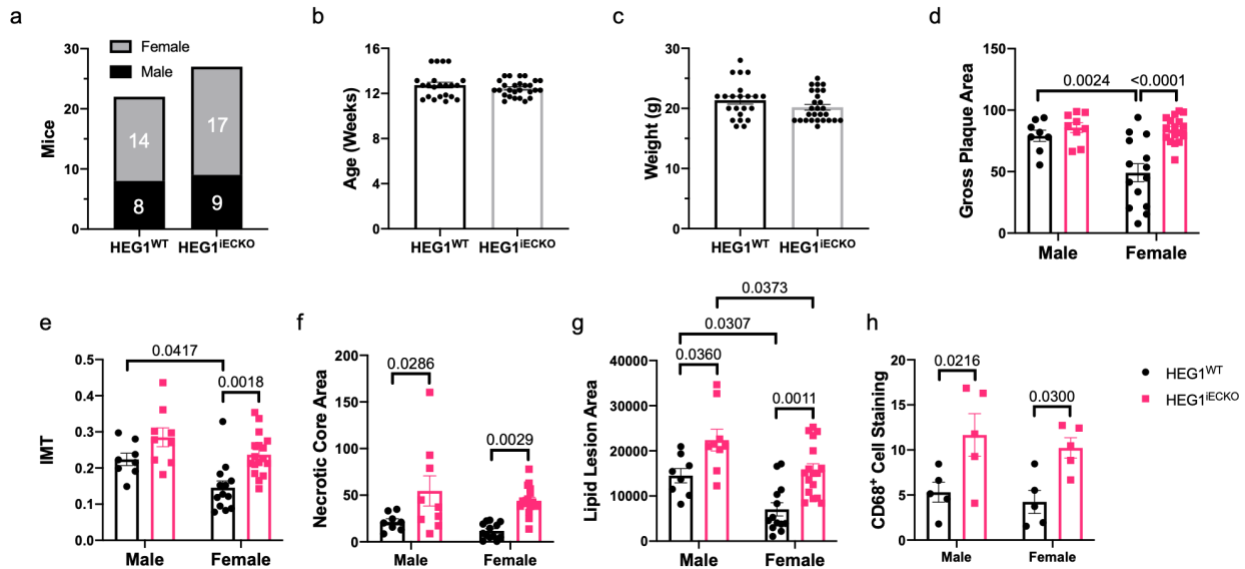


Figure 3.10 HEG1^{WT} and HEG1^{IECKO} mouse characteristics and sex-dependent atherosclerosis development

(a) 22 HEG1^{WT} (8 male, 14 female) and 27 HEG1^{IECKO} mice (9 male, 17 female) were used. Mice in both conditions had (b) equivalent ages and (c) weights at time of sacrifice. (d) Gross plaque area was equivalent in males, but increased in HEG1^{IECKO} females. WT males also had increased gross plaque as compared to WT females. (e) Intima-media thickness (IMT) was equivalent in males, but increased in HEG1^{IECKO} females. WT males again had increased IMT as compared to WT females. (f-h) HEG1^{IECKO} males and females both had increased (f) necrotic core area, (g) lipid lesion area, and (h) CD68⁺ cell infiltration as compared to WT controls. Gross plaque area quantified as percent plaque area over LCA area. IMT and necrotic core area were calculated as pixel area divided by artery length. Lipid lesion area was calculated as number of color positive pixels divided by artery length. CD68 staining is presented as average red fluorescence intensity per field.

were most noticeable in female mice, while males had more similar levels of atherosclerosis development. Nevertheless, male HEG1^{iECKO} mice had significantly increased lipid deposition, necrotic core areas, CD68 positive cell staining, indicating more advanced atherosclerotic plaque development (**Fig. 3.10d-g**). The larger, more advanced atherosclerotic plaques in the HEG1^{iECKO} mice LCAs indicate that HEG1 knockout promotes and accelerates atherogenesis, likely via EC dysfunction caused by low KLF2 and KLF4 levels. These results clearly demonstrate the atheroprotective role of HEG1.

Finally, in accordance with the decreased levels of eNOS, the HEG1^{iECKO} mice had increased blood pressure as compared to the HEG1^{WT} (**Fig. 3.9l**). Furthermore, plasma cholesterol and triglyceride levels were equivalent between the HEG1^{iECKO} and HEG1^{WT} mice, indicating that the observed changes in plaque severity were not due to differences in plasma cholesterol levels (**Fig. 3.9m**).

3.3.2 Endothelial HEG1 expression is negatively correlated with plaque severity and hypertension in human coronary arteries

Having established that increased HEG1 expression is atheroprotective, and that HEG1 levels are tightly regulated by shear stress, expression of HEG1 in ECs of human coronary arteries was evaluated. HEG1 was hypothesized to have decreased expression in ECs overlying atherosclerotic plaques as compared to the expression in ECs in regions of minimal plaque. To perform these analyses, the left anterior descending coronary (LAD) artery from donated human hearts were dissected, sectioned and stained for HEG1. Plaque severity in the LAD cross sections were graded according to AHA guidelines by three independent graders and averaged (199). First, HEG1 showed a distinct endothelial staining pattern in the LAD, confirming HEG1 enrichment in ECs as demonstrated in the scRNA-seq datasets from mice (**Fig. 3.11a**). HEG1 expression was increased in

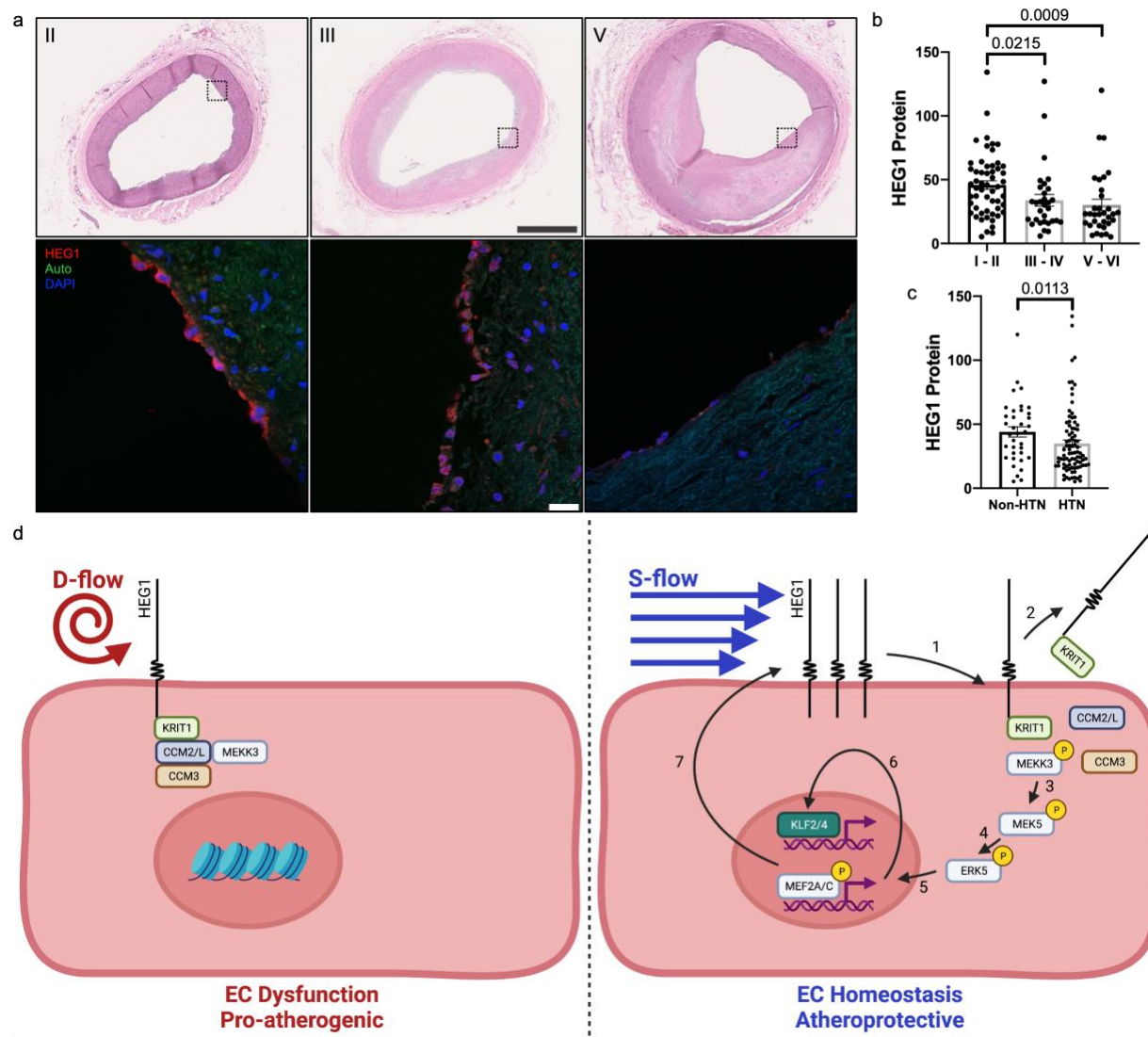


Figure 3.11 HEG1 expression is reduced with increasing plaque severity and hypertension in human coronary arteries

(a-b) HEG1 endothelial immunostaining is reduced in atherosclerotic, high plaque-grade regions as compared to healthy, low plaque-grade regions of human left anterior descending coronary arteries (scale bar top = 1 mm; scale bar bottom = 10 μ m). **(c)** HEG1 protein is reduced in coronary endothelium of hypertensive donors, as compared to non-hypertensive counterparts. **(d)** Proposed mechanism of HEG1 dynamics in d-flow and s-flow. In d-flow, low levels of HEG1 anchor KRIT1 at the apical membrane of the EC, and KRIT1 inhibits MEKK3 activation. S-flow moves HEG1 downstream of the direction of flow, and secretes HEG1 from the cell along with KRIT1, causing activation of the MEKK3-MEK5-ERK5-MEF2 pathway that induces KLF2 and KLF4 expression. KLF2 and 4 transcribe thousands of genes that control ULS-induced functional changes, EC homeostasis and atheroprotection. KLF2/4 also transcribe HEG1 mRNA to replace and enhance HEG1 protein expression in the membrane and continue MEKK3-MEK5-ERK5-MEF2 pathway activation and KLF2/4 expression in a circular feedback loop.

Type I – II plaque ECs as compared to Type III-IV and V – VI ECs, demonstrating that HEG1 expression is negatively correlated with plaque severity (**Fig. 3.11a, b**). Furthermore, HEG1 protein expression was decreased in the coronary endothelium of donors who had a history of hypertension as compared to non-hypertensive donors (**Fig. 3.11c**). These results mirror the decreased eNOS expression and increased blood pressure observed in HEG1^{iECKO} mice.

4 Discussion

4.1 Summary

Here, HEG1 is shown for the first time in mouse and human ECs to be extensively regulated by shear stress. In response to ULS, HEG1 protein moves to the downstream pole of ECs within minutes of the initiation of shear and is secreted from the cell. Over the course of several hours, HEG1 promoter region chromatin is epigenetically opened and HEG1 is transcribed by KLF2 and KLF4 to increase mRNA and protein expression. The presence of HEG1 is required to mediate ULS-induced suppression of EC inflammation, permeability, migration and tube formation. This control of shear-sensitive functional changes occurs via HEG1 control of the induction of KLF2 and KLF4, which dramatically alter the EC transcriptional profile and phenotype. HEG1 controls ULS-induced KLF2 and KLF4 induction by mediating a ULS-induced secretion of the MEKK3 inhibitor KRIT1, which allows for activation of the MEKK3-MEK5-ERK5-MEF2 pathway, resulting in KLF2 and KLF4 transcription (**Fig 3.11d**). These mechanistic insights indicate that HEG1 and KLF2/4 are involved in a circular feedback loop: in response to ULS, HEG1 is secreted from the cell with KRIT1, and induces KLF2/4 expression. To replace HEG1 in the EC plasma membrane and propagate the activity of this signaling axis, KLF2 and KLF4 transcribe HEG1.

In addition to these key mechanistic insights, HEG1 is here shown for the first time to protect against atherosclerosis. Mice lacking HEG1 showed accelerated atherosclerosis development and human coronary artery ECs showed a negative correlation between HEG1 expression and atherosclerotic plaque severity, as well as reduced HEG1 expression in donors with hypertension. These correlational results in human coronary ECs closely match a recent large-scale study of endothelial-derived proteins in the blood, which showed that circulating HEG1 levels are reduced in

individuals with atherosclerosis risk factors, including increased BMI, elevated cholesterol levels and hypertension (200).

The results of this study connect several important lines of research on HEG1, the CCM proteins and KLF2/4. Though HEG1, KRIT1 and CCM2 knockout zebrafish were found to phenocopy, HEG1 knockout or mutation was not found to cause CCM disease in mouse brains, or in humans, indicating a distinct function of HEG1 from its CCM complex binding partners (167; 168; 201; 202). Additionally, knockout of the CCM proteins, and inhibition of HEG1-KRIT1 binding have been shown repeatedly to induce KLF2 and KLF4 expression via the MEKK3-MEK5-ERK5-MEF2 pathway (194-198; 203). Previous studies focusing on CCM pathogenesis suggested that aberrantly elevated expression of KLF2/4 during development lead to the cerebral vascular anomalies characteristic of CCM disease, but have not investigated the role of this mechanism outside of development. Nevertheless the MEKK3-MEK5-ERK5-MEF2 pathway has been known for some time to be responsible for KLF2/4 induction in ULS, though the upstream regulators of this pathway have remained a mystery (124; 190-192).

With the results of the current study, it is clear that HEG1 functions as a key mediator of shear-sensitive KRIT1 protein expression, MEKK3-MEK5-ERK5-MEF2 pathway activation and KLF2/4 induction. This implies that the CCM complex, similar to several other key developmental proteins and pathways, is involved in endothelial mechano-signal transduction via its binding to HEG1 (204). The question of whether HEG1 is itself a mechanosensor, however, requires further study.

4.2 Conclusion

In conclusion, this study shows that HEG1 protects against atherosclerosis by controlling s-flow-induced KLF2/4 expression in ECs. The results of this study provide new understanding to the

function of the HEG1-CCM complex in adulthood and the process of endothelial mechanotransduction by identifying a key upstream regulator of ULS-induced KLF2/4 expression. These insights provide novel targets and strategies for the development of anti-atherogenic therapies.

4.3 Future Directions

The findings of this study lead to many interesting hypotheses that should be addressed in future research. First, further mechanistic studies must be conducted to thoroughly characterize HEG1 protein function in endothelial cells. The question of how HEG1 regulates KRIT1 and the CCM complex to activate the MEKK3-MEK5-ERK5-MEF2 pathway needs to be studied in more detail in order to describe the complex processes by which the HEG1-KRIT1-CCM complex activates MEKK3 in response to flow. Our finding that HEG1 mediates an s-flow-induced removal of KRIT1 protein from the endothelial cell is a key insight, but must be studied further.

Additionally, the findings of this study indicate that HEG1 may be a novel endothelial mechanosensor protein. Our results clearly demonstrate that HEG1 mediates endothelial mechano-signal transduction and functional responses to s-flow. Given the highly glycosylated, single-pass transmembrane structure of HEG1, similar to known mechanosensory proteins such as NOTCH1, plexin D1, the glycocalyx, and platelet mechanosensor GP1b-IX, the lack of an extracellular domain-binding ligand, and the rapid localization changes in HEG1 protein in response to s-flow, the question of whether HEG1 is a novel protein mechanosensor in endothelial cells must be addressed (205). These studies will involve the measurement of acute (seconds to minutes) endothelial flow responses following targeted mechanical stimulation of full-length and truncated mutant forms of HEG1 protein. These studies will indicate whether mechanical stimulation of the HEG1 extracellular domain is sufficient to induce canonical endothelial shear response mechano-signal transduction pathways,

and determine the function of each HEG1 protein domain in the mechanosensing and mechanotransduction process.

Another important question regarding HEG1 protein function is whether the secreted form of HEG1 that is present in conditioned media following exposure to ULS *in vitro* is a biologically active molecule. It is known that HEG1 protein circulates in the human bloodstream, and that circulating HEG1 protein levels are negatively correlated with several atherosclerosis risk factors, such as increased BMI, elevated blood cholesterol levels and high blood pressure, but the biological function of circulating HEG1 is unknown (200). To address this question, additional studies on HEG1 protein stability in the bloodstream must be conducted and the question of how HEG1 is secreted, whether in exosomes, microvesicles or an alternative form, must be addressed. Additionally, soluble, recombinant HEG1 protein could be produced and used to treat endothelial cells *in vitro*, and administered to mice in order to determine the effects of circulating HEG1 protein on endothelial and cardiovascular function.

While our PCL-induced rapid atherosclerosis studies on HEG1^{iECKO} mice clearly indicate that HEG1 protects against atherosclerosis, many additional atherosclerosis *in vivo* studies must be conducted to thoroughly characterize the atheroprotective role of HEG1. First, additional PCL studies should be conducted at time points earlier than 2 weeks in order to compare the rate of atherosclerosis development in HEG1^{WT} and HEG1^{iECKO} mice. More importantly, 4-month, chronic atherosclerosis studies on hypercholesterolemic HEG1^{WT} versus HEG1^{iECKO} mice should be performed in order to determine the effects of HEG1 KO on atherosclerosis development in a setting more analogous to human atherosclerotic disease. Extended survival studies on these mice should be conducted, as well. Furthermore, scRNA-seq analysis of HEG1^{iECKO} mouse endothelial cells should be conducted to more precisely understand the mechanisms and pathways by which HEG1 influences endothelial function and atherosclerosis, and reveal novel pathways and mechanisms of HEG1 function.

Finally, HEG1 and the CCM complex should be investigated as novel pharmacological targets to induce KLF2/4 expression in endothelial cells, thus reducing endothelial dysfunction and protecting against atherosclerosis. It is our hope that our studies lead to further understanding of endothelial function and atherogenesis, and novel therapies for the treatment of atherosclerosis.

5 References

1. Libby P, Ridker PM, Maseri A. 2002. Inflammation and atherosclerosis. *Circulation* 105:1135-43
2. Herrington W, Lacey B, Sherliker P, Armitage J, Lewington S. 2016. Epidemiology of Atherosclerosis and the Potential to Reduce the Global Burden of Atherothrombotic Disease. *Circ Res* 118:535-46
3. Davignon J, Ganz P. 2004. Role of endothelial dysfunction in atherosclerosis. *Circulation* 109:III27-32
4. Libby P. 2021. The changing landscape of atherosclerosis. *Nature* 592:524-33
5. Libby P, Ridker PM, Hansson GK, Atherothrombosis LTN. 2009. Inflammation in atherosclerosis: from pathophysiology to practice. *Journal of the American college of cardiology* 54:2129-38
6. VanderLaan PA, Reardon CA, Getz GS. 2004. Site specificity of atherosclerosis: site-selective responses to atherosclerotic modulators. *Arterioscler Thromb Vasc Biol* 24:12-22
7. Tarbell JM. 2003. Mass transport in arteries and the localization of atherosclerosis. *Annu Rev Biomed Eng* 5:79-118
8. Caro CG, Fitz-Gerald JM, Schroter RC. 1969. Arterial wall shear and distribution of early atheroma in man. *Nature* 223:1159-60
9. Ridker PM, Everett BM, Thuren T, MacFadyen JG, Chang WH, et al. 2017. Antiinflammatory Therapy with Canakinumab for Atherosclerotic Disease. *N Engl J Med* 377:1119-31
10. Topper JN, Gimbrone MA, Jr. 1999. Blood flow and vascular gene expression: fluid shear stress as a modulator of endothelial phenotype. *Mol Med Today* 5:40-6
11. Tanaka H, Shimizu S, Ohmori F, Muraoka Y, Kumagai M, et al. 2006. Increases in blood flow and shear stress to nonworking limbs during incremental exercise. *Medicine and science in sports and exercise* 38:81-5
12. Ando J, Yamamoto K. 2011. Effects of shear stress and stretch on endothelial function. *Antioxidants & redox signaling* 15:1389-403
13. Ziegler T, Bouzourene K, Harrison VJ, Brunner HR, Hayoz D. 1998. Influence of oscillatory and unidirectional flow environments on the expression of endothelin and nitric oxide synthase in cultured endothelial cells. *Arteriosclerosis, thrombosis, and vascular biology* 18:686-92
14. Balachandran K, Sucusky P, Yoganathan AP. 2011. Hemodynamics and mechanobiology of aortic valve inflammation and calcification. *International journal of inflammation* 2011
15. Andueza A, Kumar S, Kim J, Kang D-W, Mumme HL, et al. 2020. Endothelial reprogramming by disturbed flow revealed by single-cell RNA and chromatin accessibility study. *Cell reports* 33:108491
16. Cunningham KS, Gotlieb AI. 2005. The role of shear stress in the pathogenesis of atherosclerosis. *Laboratory investigation* 85:9-23

17. Simmons RD, Kumar S, Jo H. 2016. The role of endothelial mechanosensitive genes in atherosclerosis and omics approaches. *Archives of biochemistry and biophysics* 591:111-31
18. Kinlay S, Grewal J, Manuelin D, Fang JC, Selwyn AP, et al. 2002. Coronary flow velocity and disturbed flow predict adverse clinical outcome after coronary angioplasty. *Arterioscler Thromb Vasc Biol* 22:1334-40
19. Malek AM, Alper SL, Izumo S. 1999. Hemodynamic shear stress and its role in atherosclerosis. *JAMA* 282:2035-42
20. Hwang J, Ing MH, Salazar A, Lassegue B, Griendling K, et al. 2003. Pulsatile versus oscillatory shear stress regulates NADPH oxidase subunit expression: implication for native LDL oxidation. *Circ Res* 93:1225-32
21. Harrison D, Griendling KK, Landmesser U, Hornig B, Drexler H. 2003. Role of oxidative stress in atherosclerosis. *The American journal of cardiology* 91:7A-11A
22. Dewey CF, Jr., Bussolari SR, Gimbrone MA, Jr., Davies PF. 1981. The dynamic response of vascular endothelial cells to fluid shear stress. *J Biomech Eng* 103:177-85
23. Laclaustra M, Casasnovas JA, Fernandez-Ortiz A, Fuster V, Leon-Latre M, et al. 2016. Femoral and Carotid Subclinical Atherosclerosis Association With Risk Factors and Coronary Calcium: The AWHs Study. *J Am Coll Cardiol* 67:1263-74
24. Fernandez-Friera L, Penalvo JL, Fernandez-Ortiz A, Ibanez B, Lopez-Melgar B, et al. 2015. Prevalence, Vascular Distribution, and Multiterritorial Extent of Subclinical Atherosclerosis in a Middle-Aged Cohort: The PESA (Progression of Early Subclinical Atherosclerosis) Study. *Circulation* 131:2104-13
25. Chien S. 2008. Effects of disturbed flow on endothelial cells. *Annals of biomedical engineering* 36:554-62
26. Wu D, Huang RT, Hamanaka RB, Krause M, Oh MJ, et al. 2017. HIF-1alpha is required for disturbed flow-induced metabolic reprogramming in human and porcine vascular endothelium. *eLife* 6
27. Li R, Jen N, Wu L, Lee J, Fang K, et al. 2015. Disturbed Flow Induces Autophagy, but Impairs Autophagic Flux to Perturb Mitochondrial Homeostasis. *Antioxid Redox Signal* 23:1207-19
28. Baek KI, Li R, Jen N, Choi H, Kaboodrangi A, et al. 2018. Flow-Responsive Vascular Endothelial Growth Factor Receptor-Protein Kinase C Isoform Epsilon Signaling Mediates Glycolytic Metabolites for Vascular Repair. *Antioxid Redox Signal* 28:31-43
29. Nam D, Ni C-W, Rezvan A, Suo J, Budzyn K, et al. 2009. Partial carotid ligation is a model of acutely induced disturbed flow, leading to rapid endothelial dysfunction and atherosclerosis. *American Journal of Physiology-Heart and Circulatory Physiology* 297:H1535-H43
30. Cheng C, Tempel D, Van Haperen R, Van Der Baan A, Grosveld F, et al. 2006. Atherosclerotic lesion size and vulnerability are determined by patterns of fluid shear stress. *Circulation* 113:2744-53
31. Kumar S, Kang D-W, Rezvan A, Jo H. 2017. Accelerated atherosclerosis development in C57Bl6 mice by overexpressing AAV-mediated PCSK9 and partial carotid ligation. *Laboratory Investigation* 97:935-45

32. Nam D, Ni CW, Rezvan A, Suo J, Budzyn K, et al. 2010. A model of disturbed flow-induced atherosclerosis in mouse carotid artery by partial ligation and a simple method of RNA isolation from carotid endothelium. *J Vis Exp*
33. Cheng C, Tempel D, van Haperen R, van der Baan A, Grosveld F, et al. 2006. Atherosclerotic lesion size and vulnerability are determined by patterns of fluid shear stress. *Circulation* 113:2744-53
34. Sucaskey P, Padala M, Elhammali A, Balachandran K, Jo H, Yoganathan AP. 2008. Design of an ex vivo culture system to investigate the effects of shear stress on cardiovascular tissue. *J Biomech Eng* 130:035001
35. Lawrence MB, McIntire LV, Eskin SG. 1987. Effect of flow on polymorphonuclear leukocyte/endothelial cell adhesion. *Blood* 70:1284-90
36. Tang D, Geng F, Yu C, Zhang R. 2021. Recent application of zebrafish models in atherosclerosis research. *Frontiers in Cell and Developmental Biology* 9:643697
37. Schlegel A. 2016. Zebrafish models for dyslipidemia and atherosclerosis research. *Frontiers in Endocrinology* 7:159
38. Baek KI, Chang S-S, Chang C-C, Roustaei M, Ding Y, et al. 2022. Vascular Injury in the Zebrafish Tail Modulates Blood Flow and Peak Wall Shear Stress to Restore Embryonic Circular Network. *Frontiers in Cardiovascular Medicine* 9
39. Hsu JJ, Vedula V, Baek KI, Chen C, Chen J, et al. 2019. Contractile and hemodynamic forces coordinate Notch1b-mediated outflow tract valve formation. *JCI insight* 4
40. Lee J, Fei P, Packard RRS, Kang H, Xu H, et al. 2016. 4-Dimensional light-sheet microscopy to elucidate shear stress modulation of cardiac trabeculation. *The Journal of clinical investigation* 126:1679-90
41. Lee J, Vedula V, Baek KI, Chen J, Hsu JJ, et al. 2018. Spatial and temporal variations in hemodynamic forces initiate cardiac trabeculation. *JCI insight* 3
42. Tarbell JM, Shi ZD, Dunn J, Jo H. 2014. Fluid Mechanics, Arterial Disease, and Gene Expression. *Annu Rev Fluid Mech* 46:591-614
43. Rezvan A, Ni C-W, Alberts-Grill N, Jo H. 2011. Animal, in vitro, and ex vivo models of flow-dependent atherosclerosis: role of oxidative stress. *Antioxidants & redox signaling* 15:1433-48
44. Li Y-SJ, Haga JH, Chien S. 2005. Molecular basis of the effects of shear stress on vascular endothelial cells. *Journal of biomechanics* 38:1949-71
45. Berceci SA, Warty VS, Sheppeck RA, Mandarino WA, Tanksale SK, Borovetz HS. 1990. Hemodynamics and low density lipoprotein metabolism. Rates of low density lipoprotein incorporation and degradation along medial and lateral walls of the rabbit aorto-iliac bifurcation. *Arteriosclerosis* 10:686-94
46. Himburg HA, Grzybowski DM, Hazel AL, LaMack JA, Li XM, Friedman MH. 2004. Spatial comparison between wall shear stress measures and porcine arterial endothelial permeability. *Am J Physiol Heart Circ Physiol* 286:H1916-22
47. Colgan OC, Ferguson G, Collins NT, Murphy RP, Meade G, et al. 2007. Regulation of bovine brain microvascular endothelial tight junction assembly and barrier function by laminar shear stress. *Am J Physiol Heart Circ Physiol* 292:H3190-7

48. Orsenigo F, Giampietro C, Ferrari A, Corada M, Galaup A, et al. 2012. Phosphorylation of VE-cadherin is modulated by haemodynamic forces and contributes to the regulation of vascular permeability in vivo. *Nat Commun* 3:1208
49. Caolo V, Peacock HM, Kasaai B, Swennen G, Gordon E, et al. 2018. Shear Stress and VE-Cadherin. *Arterioscler Thromb Vasc Biol* 38:2174-83
50. Levesque MJ, Nerem RM, Sprague EA. 1990. Vascular endothelial cell proliferation in culture and the influence of flow. *Biomaterials* 11:702-7
51. Lin K, Hsu PP, Chen BP, Yuan S, Usami S, et al. 2000. Molecular mechanism of endothelial growth arrest by laminar shear stress. *Proc Natl Acad Sci U S A* 97:9385-9
52. Dimmeler S, Haendeler J, Rippmann V, Nehls M, Zeiher AM. 1996. Shear stress inhibits apoptosis of human endothelial cells. *FEBS Lett* 399:71-4
53. Dimmeler S, Assmus B, Hermann C, Haendeler J, Zeiher AM. 1998. Fluid shear stress stimulates phosphorylation of Akt in human endothelial cells: involvement in suppression of apoptosis. *Circ Res* 83:334-41
54. Liu J, Bi X, Chen T, Zhang Q, Wang S, et al. 2015. Shear stress regulates endothelial cell autophagy via redox regulation and Sirt1 expression. *Cell death & disease* 6:e1827-e
55. Warboys CM, de Luca A, Amini N, Luong L, Duckles H, et al. 2014. Disturbed flow promotes endothelial senescence via a p53-dependent pathway. *Arteriosclerosis, thrombosis, and vascular biology* 34:985-95
56. Doddaballapur A, Michalik KM, Manavski Y, Lucas T, Houtkooper RH, et al. 2015. Laminar shear stress inhibits endothelial cell metabolism via KLF2-mediated repression of PFKFB3. *Arterioscler Thromb Vasc Biol* 35:137-45
57. Yamamoto K, Imamura H, Ando J. 2018. Shear stress augments mitochondrial ATP generation that triggers ATP release and Ca(2+) signaling in vascular endothelial cells. *Am J Physiol Heart Circ Physiol* 315:H1477-H85
58. Go YM, Kim CW, Walker DI, Kang DW, Kumar S, et al. 2015. Disturbed flow induces systemic changes in metabolites in mouse plasma: a metabolomics study using ApoE(-)/(-) mice with partial carotid ligation. *Am J Physiol Regul Integr Comp Physiol* 308:R62-72
59. Hong SG, Shin J, Choi SY, Powers JC, Meister BM, et al. 2022. Flow pattern-dependent mitochondrial dynamics regulates the metabolic profile and inflammatory state of endothelial cells. *JCI Insight* 7
60. Heo K-S, Fujiwara K, Abe J-i. 2011. Disturbed-flow-mediated vascular reactive oxygen species induce endothelial dysfunction. *Circulation Journal* 75:2722-30
61. Zhang JX, Qu XL, Chu P, Xie DJ, Zhu LL, et al. 2018. Low shear stress induces vascular eNOS uncoupling via autophagy-mediated eNOS phosphorylation. *Biochim Biophys Acta Mol Cell Res* 1865:709-20
62. Jo H, Song H, Mowbray A. 2006. Role of NADPH oxidases in disturbed flow-and BMP4-induced inflammation and atherosclerosis. *Antioxidants & redox signaling* 8:1609-19
63. Sorescu GP, Song H, Tressel SL, Hwang J, Dikalov S, et al. 2004. Bone morphogenic protein 4 produced in endothelial cells by oscillatory shear stress induces monocyte adhesion by stimulating reactive oxygen species production from a nox1-based NADPH oxidase. *Circulation research* 95:773-9

64. Go Y-M, Levenon A-L, Moellering D, Ramachandran A, Patel RP, et al. 2001. Endothelial NOS-dependent activation of c-Jun NH2-terminal kinase by oxidized low-density lipoprotein. *American Journal of Physiology-Heart and Circulatory Physiology* 281:H2705-H13
65. Nagel T, Resnick N, Dewey CF, Jr., Gimbrone MA, Jr. 1999. Vascular endothelial cells respond to spatial gradients in fluid shear stress by enhanced activation of transcription factors. *Arterioscler Thromb Vasc Biol* 19:1825-34
66. Sterpetti AV, Cucina A, Morena AR, Di Donna S, D'Angelo LS, et al. 1993. Shear stress increases the release of interleukin-1 and interleukin-6 by aortic endothelial cells. *Surgery* 114:911-4
67. Souilhol C, Harmsen MC, Evans PC, Krenning G. 2018. Endothelial–mesenchymal transition in atherosclerosis. *Cardiovascular research* 114:565-77
68. Takabe W, Alberts-Grill N, Jo H. 2011. Disturbed flow: p53 SUMOylation in the turnover of endothelial cells. *Journal of Cell Biology* 193:805-7
69. Flaherty JT, Pierce JE, Ferrans VJ, Patel DJ, Tucker WK, Fry DL. 1972. Endothelial nuclear patterns in the canine arterial tree with particular reference to hemodynamic events. *Circ Res* 30:23-33
70. Nerem RM, Levesque MJ, Cornhill JF. 1981. Vascular endothelial morphology as an indicator of the pattern of blood flow. *J Biomech Eng* 103:172-6
71. Langille BL, Adamson SL. 1981. Relationship between blood flow direction and endothelial cell orientation at arterial branch sites in rabbits and mice. *Circ Res* 48:481-8
72. Franke RP, Grafe M, Schnittler H, Seiffge D, Mittermayer C, Drenckhahn D. 1984. Induction of human vascular endothelial stress fibres by fluid shear stress. *Nature* 307:648-9
73. Kim DW, Langille BL, Wong MK, Gotlieb AI. 1989. Patterns of endothelial microfilament distribution in the rabbit aorta in situ. *Circ Res* 64:21-31
74. Tzima E, Irani-Tehrani M, Kiosses WB, Dejana E, Schultz DA, et al. 2005. A mechanosensory complex that mediates the endothelial cell response to fluid shear stress. *Nature* 437:426-31
75. Steward R, Jr., Tambe D, Hardin CC, Krishnan R, Fredberg JJ. 2015. Fluid shear, intercellular stress, and endothelial cell alignment. *Am J Physiol Cell Physiol* 308:C657-64
76. Galbraith C, Skalak R, Chien S. 1998. Shear stress induces spatial reorganization of the endothelial cell cytoskeleton. *Cell motility and the cytoskeleton* 40:317-30
77. Coan DE, Wechezak AR, Viggers RF, Sauvage LR. 1993. Effect of shear stress upon localization of the Golgi apparatus and microtubule organizing center in isolated cultured endothelial cells. *Journal of Cell Science* 104:1145-53
78. Demos C, Tamargo I, Jo H. 2021. Biomechanical regulation of endothelial function in atherosclerosis. *Biomechanics of Coronary Atherosclerotic Plaque*:3-47
79. Boo YC, Hwang J, Sykes M, Michell BJ, Kemp BE, et al. 2002. Shear stress stimulates phosphorylation of eNOS at Ser(635) by a protein kinase A-dependent mechanism. *Am J Physiol Heart Circ Physiol* 283:H1819-28
80. Tzima E, del Pozo MA, Shattil SJ, Chien S, Schwartz MA. 2001. Activation of integrins in endothelial cells by fluid shear stress mediates Rho-dependent cytoskeletal alignment. *EMBO J* 20:4639-47

81. Mehta V, Pang KL, Rozbesky D, Nather K, Keen A, et al. 2020. The guidance receptor plexin D1 is a mechanosensor in endothelial cells. *Nature* 578:290-5
82. Ridone P, Vassalli M, Martinac B. 2019. Piezo1 mechanosensitive channels: what are they and why are they important. *Biophys Rev* 11:795-805
83. Li J, Hou B, Tumova S, Muraki K, Bruns A, et al. 2014. Piezo1 integration of vascular architecture with physiological force. *Nature* 515:279-82
84. Ranade SS, Qiu Z, Woo SH, Hur SS, Murthy SE, et al. 2014. Piezo1, a mechanically activated ion channel, is required for vascular development in mice. *Proc Natl Acad Sci U S A* 111:10347-52
85. Zheng Q, Zou Y, Teng P, Chen Z, Wu Y, et al. 2022. Mechanosensitive Channel PIEZO1 Senses Shear Force to Induce KLF2/4 Expression via CaMKII/MEKK3/ERK5 Axis in Endothelial Cells. *Cells* 11
86. Mack JJ, Mosqueiro TS, Archer BJ, Jones WM, Sunshine H, et al. 2017. NOTCH1 is a mechanosensor in adult arteries. *Nat Commun* 8:1620
87. Chachisvilis M, Zhang YL, Frangos JA. 2006. G protein-coupled receptors sense fluid shear stress in endothelial cells. *Proc Natl Acad Sci U S A* 103:15463-8
88. Xu J, Mathur J, Vessieres E, Hammack S, Nonomura K, et al. 2018. GPR68 Senses Flow and Is Essential for Vascular Physiology. *Cell* 173:762-75 e16
89. Florian JA, Kosky JR, Ainslie K, Pang Z, Dull RO, Tarbell JM. 2003. Heparan sulfate proteoglycan is a mechanosensor on endothelial cells. *Circ Res* 93:e136-42
90. Bartosch AMW, Mathews R, Tarbell JM. 2017. Endothelial Glycocalyx-Mediated Nitric Oxide Production in Response to Selective AFM Pulling. *Biophys J* 113:101-8
91. Nauli SM, Kawanabe Y, Kaminski JJ, Pearce WJ, Ingber DE, Zhou J. 2008. Endothelial cilia are fluid shear sensors that regulate calcium signaling and nitric oxide production through polycystin-1. *Circulation* 117:1161-71
92. Shin H, Haga JH, Kosawada T, Kimura K, Li YS, et al. 2019. Fine control of endothelial VEGFR-2 activation: caveolae as fluid shear stress shelters for membrane receptors. *Biomech Model Mechanobiol* 18:5-16
93. Su Y, Xia W, Li J, Walz T, Humphries MJ, et al. 2016. Relating conformation to function in integrin alpha5beta1. *Proc Natl Acad Sci U S A* 113:E3872-81
94. Schwarz US, Gardel ML. 2012. United we stand—integrating the actin cytoskeleton and cell–matrix adhesions in cellular mechanotransduction. *Journal of cell science* 125:3051-60
95. Christensen AP, Corey DP. 2007. TRP channels in mechanosensation: direct or indirect activation? *Nat Rev Neurosci* 8:510-21
96. Murthy SE, Dubin AE, Patapoutian A. 2017. Piezos thrive under pressure: mechanically activated ion channels in health and disease. *Nat Rev Mol Cell Biol* 18:771-83
97. Wang S, Chennupati R, Kaur H, Iring A, Wettschureck N, Offermanns S. 2016. Endothelial cation channel PIEZO1 controls blood pressure by mediating flow-induced ATP release. *J Clin Invest* 126:4527-36
98. Wang S, Iring A, Strilic B, Albarran Juarez J, Kaur H, et al. 2015. P2Y(2) and Gq/G(1)(1) control blood pressure by mediating endothelial mechanotransduction. *J Clin Invest* 125:3077-86

99. Iring A, Jin YJ, Albarran-Juarez J, Siragusa M, Wang S, et al. 2019. Shear stress-induced endothelial adrenomedullin signaling regulates vascular tone and blood pressure. *J Clin Invest* 129:2775-91
100. Albarrán-Juárez J, Iring A, Wang S, Joseph S, Grimm M, et al. 2018. Piezo1 and Gq/G11 promote endothelial inflammation depending on flow pattern and integrin activation. *Journal of Experimental Medicine* 215:2655-72
101. Komarova YA, Kruse K, Mehta D, Malik AB. 2017. Protein interactions at endothelial junctions and signaling mechanisms regulating endothelial permeability. *Circulation research* 120:179-206
102. Harry BL, Sanders JM, Feaver RE, Lansey M, Deem TL, et al. 2008. Endothelial cell PECAM-1 promotes atherosclerotic lesions in areas of disturbed flow in ApoE-deficient mice. *Arteriosclerosis, thrombosis, and vascular biology* 28:2003-8
103. Stupack DG, Cheresch DA. 2002. ECM remodeling regulates angiogenesis: endothelial integrins look for new ligands. *Sci STKE* 2002:pe7
104. Tzima E. 2006. Role of small GTPases in endothelial cytoskeletal dynamics and the shear stress response. *Circ Res* 98:176-85
105. Wang L, Luo JY, Li B, Tian XY, Chen LJ, et al. 2016. Integrin-YAP/TAZ-JNK cascade mediates atheroprotective effect of unidirectional shear flow. *Nature* 540:579-82
106. Civelekoglu-Scholey G, Orr AW, Novak I, Meister JJ, Schwartz MA, Mogilner A. 2005. Model of coupled transient changes of Rac, Rho, adhesions and stress fibers alignment in endothelial cells responding to shear stress. *J Theor Biol* 232:569-85
107. Tzima E, Kiosses WB, del Pozo MA, Schwartz MA. 2003. Localized cdc42 activation, detected using a novel assay, mediates microtubule organizing center positioning in endothelial cells in response to fluid shear stress. *J Biol Chem* 278:31020-3
108. Palazzo AF, Joseph HL, Chen YJ, Dujardin DL, Alberts AS, et al. 2001. Cdc42, dynein, and dynactin regulate MTOC reorientation independent of Rho-regulated microtubule stabilization. *Curr Biol* 11:1536-41
109. Orr AW, Sanders JM, Bevard M, Coleman E, Sarembock IJ, Schwartz MA. 2005. The subendothelial extracellular matrix modulates NF-kappaB activation by flow: a potential role in atherosclerosis. *J Cell Biol* 169:191-202
110. Chen J, Green J, Yurdagul A, Jr., Albert P, McInnis MC, Orr AW. 2015. alphavbeta3 Integrins Mediate Flow-Induced NF-kappaB Activation, Proinflammatory Gene Expression, and Early Atherogenic Inflammation. *Am J Pathol* 185:2575-89
111. Li B, He J, Lv H, Liu Y, Lv X, et al. 2019. c-Abl regulates YAPY357 phosphorylation to activate endothelial atherogenic responses to disturbed flow. *J Clin Invest* 129:1167-79
112. Dekker RJ, van Thienen JV, Rohlena J, de Jager SC, Elderkamp YW, et al. 2005. Endothelial KLF2 links local arterial shear stress levels to the expression of vascular tone-regulating genes. *Am J Pathol* 167:609-18
113. Lin Z, Kumar A, SenBanerjee S, Staniszewski K, Parmar K, et al. 2005. Kruppel-like factor 2 (KLF2) regulates endothelial thrombotic function. *Circ Res* 96:e48-57
114. van Thienen JV, Fledderus JO, Dekker RJ, Rohlena J, van Ijzendoorn GA, et al. 2006. Shear stress sustains atheroprotective endothelial KLF2 expression more potently than statins through mRNA stabilization. *Cardiovasc Res* 72:231-40

115. Young A, Wu W, Sun W, Benjamin Larman H, Wang N, et al. 2009. Flow activation of AMP-activated protein kinase in vascular endothelium leads to Kruppel-like factor 2 expression. *Arterioscler Thromb Vasc Biol* 29:1902-8
116. Wu C, Huang RT, Kuo CH, Kumar S, Kim CW, et al. 2015. Mechanosensitive PPAP2B Regulates Endothelial Responses to Atherorelevant Hemodynamic Forces. *Circ Res* 117:e41-e53
117. SenBanerjee S, Lin ZY, Atkins GB, Greif DM, Rao RM, et al. 2004. KLF2 is a novel transcriptional regulator of endothelial proinflammatory activation. *Journal of Experimental Medicine* 199:1305-15
118. Hsieh CY, Hsiao HY, Wu WY, Liu CA, Tsai YC, et al. 2009. Regulation of shear-induced nuclear translocation of the Nrf2 transcription factor in endothelial cells. *J Biomed Sci* 16:12
119. Fledderus JO, Boon RA, Volger OL, Hurttila H, Yla-Herttuala S, et al. 2008. KLF2 primes the antioxidant transcription factor Nrf2 for activation in endothelial cells. *Arterioscler Thromb Vasc Biol* 28:1339-46
120. Berk BC. 2008. Atheroprotective signaling mechanisms activated by steady laminar flow in endothelial cells. *Circulation* 117:1082-9
121. Abe J, Berk BC. 2014. Novel mechanisms of endothelial mechanotransduction. *Arterioscler Thromb Vasc Biol* 34:2378-86
122. Kasler HG, Victoria J, Duramad O, Winoto A. 2000. ERK5 is a novel type of mitogen-activated protein kinase containing a transcriptional activation domain. *Mol Cell Biol* 20:8382-9
123. Sohn SJ, Li D, Lee LK, Winoto A. 2005. Transcriptional regulation of tissue-specific genes by the ERK5 mitogen-activated protein kinase. *Mol Cell Biol* 25:8553-66
124. Parmar KM, Larman HB, Dai G, Zhang Y, Wang ET, et al. 2006. Integration of flow-dependent endothelial phenotypes by Kruppel-like factor 2. *J Clin Invest* 116:49-58
125. Woo CH, Massett MP, Shishido T, Itoh S, Ding B, et al. 2006. ERK5 activation inhibits inflammatory responses via peroxisome proliferator-activated receptor delta (PPARdelta) stimulation. *J Biol Chem* 281:32164-74
126. Akaike M, Che W, Marmarosh NL, Ohta S, Osawa M, et al. 2004. The hinge-helix 1 region of peroxisome proliferator-activated receptor gamma1 (PPARGgamma1) mediates interaction with extracellular signal-regulated kinase 5 and PPARGgamma1 transcriptional activation: involvement in flow-induced PPARGgamma activation in endothelial cells. *Mol Cell Biol* 24:8691-704
127. Woo CH, Shishido T, McClain C, Lim JH, Li JD, et al. 2008. Extracellular signal-regulated kinase 5 SUMOylation antagonizes shear stress-induced antiinflammatory response and endothelial nitric oxide synthase expression in endothelial cells. *Circ Res* 102:538-45
128. Mohan S, Mohan N, Sprague EA. 1997. Differential activation of NF-kappa B in human aortic endothelial cells conditioned to specific flow environments. *Am J Physiol* 273:C572-8
129. Nakajima H, Mochizuki N. 2017. Flow pattern-dependent endothelial cell responses through transcriptional regulation. *Cell Cycle* 16:1893-901

130. Kempe S, Kestler H, Lasar A, Wirth T. 2005. NF-kappaB controls the global pro-inflammatory response in endothelial cells: evidence for the regulation of a pro-atherogenic program. *Nucleic Acids Res* 33:5308-19
131. van Uden P, Kenneth NS, Rocha S. 2008. Regulation of hypoxia-inducible factor-1alpha by NF-kappaB. *Biochem J* 412:477-84
132. Mohan S, Mohan N, Sprague EA. 1997. Differential activation of NF-kappa B in human aortic endothelial cells conditioned to specific flow environments. *American Journal of Physiology-Cell Physiology* 273:C572-C8
133. Feng S, Bowden N, Fragiadaki M, Souilhol C, Hsiao S, et al. 2017. Mechanical Activation of Hypoxia-Inducible Factor 1alpha Drives Endothelial Dysfunction at Atheroprone Sites. *Arterioscler Thromb Vasc Biol* 37:2087-101
134. Ajami NE, Gupta S, Maurya MR, Nguyen P, Li JY-S, et al. 2017. Systems biology analysis of longitudinal functional response of endothelial cells to shear stress. *Proceedings of the National Academy of Sciences* 114:10990-5
135. Villa-Roel N, Ryu K, Gu L, Fernandez Esmerats J, Kang DW, et al. 2022. Hypoxia inducible factor 1alpha inhibitor PX-478 reduces atherosclerosis in mice. *Atherosclerosis* 344:20-30
136. Wu D, Huang RT, Hamanaka RB, Krause M, Oh MJ, et al. 2017. HIF-1 alpha is required for disturbed flow-induced metabolic reprogramming in human and porcine vascular endothelium. *Elife* 6
137. Wang K-C, Yeh Y-T, Nguyen P, Limqueco E, Lopez J, et al. 2016. Flow-dependent YAP/TAZ activities regulate endothelial phenotypes and atherosclerosis. *Proceedings of the National Academy of Sciences* 113:11525-30
138. Zanconato F, Cordenonsi M, Piccolo S. 2016. YAP/TAZ at the roots of cancer. *Cancer cell* 29:783-803
139. Piccolo S, Dupont S, Cordenonsi M. 2014. The biology of YAP/TAZ: hippo signaling and beyond. *Physiological reviews*
140. Demos C, Johnson J, Andueza A, Park C, Kim Y, et al. 2022. Sox13 is a novel flow-sensitive transcription factor that prevents inflammation by repressing chemokine expression in endothelial cells. *Front Cardiovasc Med* 9:979745
141. Ni C-W, Qiu H, Rezvan A, Kwon K, Nam D, et al. 2010. Discovery of novel mechanosensitive genes in vivo using mouse carotid artery endothelium exposed to disturbed flow. *Blood, The Journal of the American Society of Hematology* 116:e66-e73
142. Dunn J, Qiu H, Kim S, Jjingo D, Hoffman R, et al. 2014. Flow-dependent epigenetic DNA methylation regulates endothelial gene expression and atherosclerosis. *The Journal of clinical investigation* 124:3187-99
143. Chen X, Liu L, Palacios G, Gao J, Zhang N, et al. 2010. Plasma metabolomics reveals biomarkers of the atherosclerosis. *Journal of separation science* 33:2776-83
144. Goveia J, Stapor P, Carmeliet P. 2014. Principles of targeting endothelial cell metabolism to treat angiogenesis and endothelial cell dysfunction in disease. *EMBO molecular medicine* 6:1105-20
145. Wu J, Liu W, Sousa E, Qiu Y, Pittman DD, et al. 2007. Proteomic identification of endothelial proteins isolated in situ from atherosclerotic aorta via systemic perfusion. *Journal of Proteome Research* 6:4728-36

146. Kumar S, Williams D, Sur S, Wang J-Y, Jo H. 2019. Role of flow-sensitive microRNAs and long noncoding RNAs in vascular dysfunction and atherosclerosis. *Vascular pharmacology* 114:76-92
147. Simmons RD, Kumar S, Thabet SR, Sur S, Jo H. 2016. Omics-based approaches to understand mechanosensitive endothelial biology and atherosclerosis. *Wiley Interdisciplinary Reviews: Systems Biology and Medicine* 8:378-401
148. Williams D, Mahmoud M, Liu R, Andueza A, Kumar S, et al. 2022. Stable flow-induced expression of KLK10 inhibits endothelial inflammation and atherosclerosis. *Elife* 11
149. Liu R, Qu S, Xu Y, Jo H, Dai Z. 2022. Spatial control of robust transgene expression in mouse artery endothelium under ultrasound guidance. *Signal Transduction and Targeted Therapy* 7:1-3
150. Villarreal Jr G, Zhang Y, Larman HB, Gracia-Sancho J, Koo A, García-Cardena G. 2010. Defining the regulation of KLF4 expression and its downstream transcriptional targets in vascular endothelial cells. *Biochemical and biophysical research communications* 391:984-9
151. Zhou J, Li Y-S, Wang K-C, Chien S. 2014. Epigenetic mechanism in regulation of endothelial function by disturbed flow: induction of DNA hypermethylation by DNMT1. *Cellular and molecular bioengineering* 7:218-24
152. Firasat S, Hecker M, Binder L, Asif AR. 2014. Advances in endothelial shear stress proteomics. *Expert review of proteomics* 11:611-9
153. Burghoff S, Schrader Jr. 2011. Secretome of human endothelial cells under shear stress. *Journal of Proteome Research* 10:1160-9
154. Bibli S-I, Hu J, Sigala F, Wittig I, Heidler J, et al. 2019. Cystathionine γ lyase sulfhydrates the RNA binding protein human antigen R to preserve endothelial cell function and delay atherogenesis. *Circulation* 139:101-14
155. Parmar KM, Nambudiri V, Dai G, Larman HB, Gimbrone MA, Jr., Garcia-Cardena G. 2005. Statins exert endothelial atheroprotective effects via the KLF2 transcription factor. *J Biol Chem* 280:26714-9
156. Kumar S, Sur S, Perez J, Demos C, Kang DW, et al. 2021. Atorvastatin and blood flow regulate expression of distinctive sets of genes in mouse carotid artery endothelium. *Curr Top Membr* 87:97-130
157. Parmar KM, Nambudiri V, Dai G, Larman HB, Gimbrone MA, García-Cardena G. 2005. Statins exert endothelial atheroprotective effects via the KLF2 transcription factor. *Journal of Biological Chemistry* 280:26714-9
158. Lee GH, Park JS, Jin SW, Pham TH, Thai TN, et al. 2020. Betulinic Acid Induces eNOS Expression via the AMPK-Dependent KLF2 Signaling Pathway. *J Agric Food Chem* 68:14523-30
159. Davies JE, Lopresto D, Apta BHR, Lin Z, Ma W, Harper MT. 2019. Using Yoda-1 to mimic laminar flow in vitro: A tool to simplify drug testing. *Biochem Pharmacol* 168:473-80
160. Syeda R, Xu J, Dubin AE, Coste B, Mathur J, et al. 2015. Chemical activation of the mechanotransduction channel Piezo1. *Elife* 4
161. Wang Y, Chi S, Guo H, Li G, Wang L, et al. 2018. A lever-like transduction pathway for long-distance chemical- and mechano-gating of the mechanosensitive Piezo1 channel. *Nat Commun* 9:1300

162. Son DJ, Kumar S, Takabe W, Woo Kim C, Ni C-W, et al. 2013. The atypical mechanosensitive microRNA-712 derived from pre-ribosomal RNA induces endothelial inflammation and atherosclerosis. *Nature communications* 4:1-15
163. Wu W, Xiao H, Laguna-Fernandez A, Villarreal Jr G, Wang K-C, et al. 2011. Flow-dependent regulation of Krüppel-like factor 2 is mediated by microRNA-92a. *Circulation* 124:633-41
164. Kim CW, Kumar S, Son DJ, Jang I-H, Griendling KK, Jo H. 2014. Prevention of abdominal aortic aneurysm by Anti-MicroRNA-712 or Anti-MicroRNA-205 in angiotensin II-infused mice. *Arteriosclerosis, thrombosis, and vascular biology* 34:1412-21
165. Nam D, Ni CW, Rezvan A, Suo J, Budzyn K, et al. 2009. Partial carotid ligation is a model of acutely induced disturbed flow, leading to rapid endothelial dysfunction and atherosclerosis. *Am J Physiol Heart Circ Physiol* 297:H1535-43
166. Kleaveland B, Zheng X, Liu JJ, Blum Y, Tung JJ, et al. 2009. Regulation of cardiovascular development and integrity by the heart of glass-cerebral cavernous malformation protein pathway. *Nat Med* 15:169-76
167. Mably JD, Mohideen MA, Burns CG, Chen JN, Fishman MC. 2003. heart of glass regulates the concentric growth of the heart in zebrafish. *Curr Biol* 13:2138-47
168. Stainier DY, Fouquet B, Chen JN, Warren KS, Weinstein BM, et al. 1996. Mutations affecting the formation and function of the cardiovascular system in the zebrafish embryo. *Development* 123:285-92
169. Gingras AR, Liu JJ, Ginsberg MH. 2012. Structural basis of the junctional anchorage of the cerebral cavernous malformations complex. *J Cell Biol* 199:39-48
170. Gingras AR, Puzon-McLaughlin W, Ginsberg MH. 2013. The structure of the ternary complex of Krev interaction trapped 1 (KRIT1) bound to both the Rap1 GTPase and the heart of glass (HEG1) cytoplasmic tail. *J Biol Chem* 288:23639-49
171. Spiegler S, Najm J, Liu J, Gkalympoudis S, Schroder W, et al. 2014. High mutation detection rates in cerebral cavernous malformation upon stringent inclusion criteria: one-third of probands are minors. *Mol Genet Genomic Med* 2:176-85
172. Glading A, Han J, Stockton RA, Ginsberg MH. 2007. KRIT-1/CCM1 is a Rap1 effector that regulates endothelial cell cell junctions. *J Cell Biol* 179:247-54
173. Glading AJ, Ginsberg MH. 2010. Rap1 and its effector KRIT1/CCM1 regulate beta-catenin signaling. *Dis Model Mech* 3:73-83
174. de Kreuk BJ, Gingras AR, Knight JD, Liu JJ, Gingras AC, Ginsberg MH. 2016. Heart of glass anchors Rasip1 at endothelial cell-cell junctions to support vascular integrity. *Elife* 5:e11394
175. Andueza A, Kumar S, Kim J, Kang DW, Mumme HL, et al. 2020. Endothelial Reprogramming by Disturbed Flow Revealed by Single-Cell RNA and Chromatin Accessibility Study. *Cell Rep* 33:108491
176. Ni CW, Qiu H, Rezvan A, Kwon K, Nam D, et al. 2010. Discovery of novel mechanosensitive genes in vivo using mouse carotid artery endothelium exposed to disturbed flow. *Blood* 116:e66-73
177. Maciag T, Cerundolo J, Ilsley S, Kelley PR, Forand R. 1979. An endothelial cell growth factor from bovine hypothalamus: identification and partial characterization. *Proc Natl Acad Sci U S A* 76:5674-8

178. Matsuura R, Kaji H, Tomioka A, Sato T, Narimatsu H, et al. 2018. Identification of mesothelioma-specific sialylated epitope recognized with monoclonal antibody SKM9-2 in a mucin-like membrane protein HEG1. *Sci Rep* 8:14251
179. Tsuji S, Washimi K, Kageyama T, Yamashita M, Yoshihara M, et al. 2017. HEG1 is a novel mucin-like membrane protein that serves as a diagnostic and therapeutic target for malignant mesothelioma. *Sci Rep* 7:45768
180. Son DJ, Kumar S, Takabe W, Kim CW, Ni CW, et al. 2013. The atypical mechanosensitive microRNA-712 derived from pre-ribosomal RNA induces endothelial inflammation and atherosclerosis. *Nat Commun* 4:3000
181. Dubrovskiy O, Birukova AA, Birukov KG. 2013. Measurement of local permeability at subcellular level in cell models of agonist- and ventilator-induced lung injury. *Lab Invest* 93:254-63
182. Tressel SL, Huang RP, Tomsen N, Jo H. 2007. Laminar shear inhibits tubule formation and migration of endothelial cells by an angiopoietin-2 dependent mechanism. *Arterioscler Thromb Vasc Biol* 27:2150-6
183. Liang CC, Park AY, Guan JL. 2007. In vitro scratch assay: a convenient and inexpensive method for analysis of cell migration in vitro. *Nat Protoc* 2:329-33
184. Wang Y, Nakayama M, Pitulescu ME, Schmidt TS, Bochenek ML, et al. 2010. Ephrin-B2 controls VEGF-induced angiogenesis and lymphangiogenesis. *Nature* 465:483-6
185. Kumar S, Kang DW, Rezvan A, Jo H. 2017. Accelerated atherosclerosis development in C57Bl6 mice by overexpressing AAV-mediated PCSK9 and partial carotid ligation. *Lab Invest* 97:935-45
186. Berg S, Kutra D, Kroeger T, Straehle CN, Kausler BX, et al. 2019. ilastik: interactive machine learning for (bio)image analysis. *Nat Methods* 16:1226-32
187. Chang K, Weiss D, Suo J, Vega JD, Giddens D, et al. 2007. Bone Morphogenic Protein Antagonists Are Coexpressed With Bone Morphogenic Protein 4 in Endothelial Cells Exposed to Unstable Flow In Vitro in Mouse Aortas and in Human Coronary Arteries. *Circulation* 116:1258-66
188. Stary HC, Chandler AB, Dinsmore RE, Fuster V, Glagov S, et al. 1995. A definition of advanced types of atherosclerotic lesions and a histological classification of atherosclerosis. A report from the Committee on Vascular Lesions of the Council on Arteriosclerosis, American Heart Association. *Arterioscler Thromb Vasc Biol* 15:1512-31
189. Donat S, Lourenco M, Paolini A, Otten C, Renz M, Abdelilah-Seyfried S. 2018. Heg1 and Ccm1/2 proteins control endocardial mechanosensitivity during zebrafish valvulogenesis. *Elife* 7
190. Atkins GB, Jain MK. 2007. Role of Kruppel-like transcription factors in endothelial biology. *Circ Res* 100:1686-95
191. Clark PR, Jensen TJ, Kluger MS, Morelock M, Hanidu A, et al. 2011. MEK5 is activated by shear stress, activates ERK5 and induces KLF4 to modulate TNF responses in human dermal microvascular endothelial cells. *Microcirculation* 18:102-17
192. Ohnesorge N, Viemann D, Schmidt N, Czymai T, Spiering D, et al. 2010. Erk5 activation elicits a vasoprotective endothelial phenotype via induction of Kruppel-like factor 4 (KLF4). *J Biol Chem* 285:26199-210

193. de Kreuk B-J, Gingras AR, Knight JDR, Liu JJ, Gingras A-C, Ginsberg MH. 2016. Heart of glass anchors Rasip1 at endothelial cell-cell junctions to support vascular integrity. *eLife* 5:e11394
194. Zhou Z, Tang AT, Wong WY, Bamezai S, Goddard LM, et al. 2016. Cerebral cavernous malformations arise from endothelial gain of MEKK3-KLF2/4 signalling. *Nature* 532:122-6
195. Cuttano R, Rudini N, Bravi L, Corada M, Giampietro C, et al. 2016. KLF4 is a key determinant in the development and progression of cerebral cavernous malformations. *EMBO Mol Med* 8:6-24
196. Zhou Z, Rawnsley DR, Goddard LM, Pan W, Cao XJ, et al. 2015. The cerebral cavernous malformation pathway controls cardiac development via regulation of endocardial MEKK3 signaling and KLF expression. *Dev Cell* 32:168-80
197. Cullere X, Plovie E, Bennett PM, MacRae CA, Mayadas TN. 2015. The cerebral cavernous malformation proteins CCM2L and CCM2 prevent the activation of the MAP kinase MEKK3. *Proc Natl Acad Sci U S A* 112:14284-9
198. Fisher OS, Deng H, Liu D, Zhang Y, Wei R, et al. 2015. Structure and vascular function of MEKK3-cerebral cavernous malformations 2 complex. *Nat Commun* 6:7937
199. Strydom HC, Chandler AB, Dinsmore RE, Fuster V, Glagov S, et al. 1995. A definition of advanced types of atherosclerotic lesions and a histological classification of atherosclerosis. A report from the Committee on Vascular Lesions of the Council on Arteriosclerosis, American Heart Association. *Circulation* 92:1355-74
200. Iglesias MJ, Kruse LD, Sanchez-Rivera L, Enge L, Dusart P, et al. 2021. Identification of Endothelial Proteins in Plasma Associated With Cardiovascular Risk Factors. *Arterioscler Thromb Vasc Biol* 41:2990-3004
201. Mably JD, Chuang LP, Serluca FC, Mohideen MA, Chen JN, Fishman MC. 2006. Santa and valentine pattern concentric growth of cardiac myocardium in the zebrafish. *Development* 133:3139-46
202. Zheng X, Riant F, Bergametti F, Myers CD, Tang AT, et al. 2014. Cerebral cavernous malformations arise independent of the heart of glass receptor. *Stroke* 45:1505-9
203. Lopez-Ramirez MA, Haynes MK, Hale P, O'ukoloff K, Bautista M, et al. 2019. Pharmacological inhibition of the heart of glass (HEG1)-Krev interaction trapped protein 1 (KRIT1) protein complex increases Krüppel-like Factors 4 and 2 (KLF4/2) expression in endothelial cells. *bioRxiv*
204. Souilhol C, Serbanovic-Canic J, Fragiadaki M, Chico TJ, Ridger V, et al. 2020. Endothelial responses to shear stress in atherosclerosis: a novel role for developmental genes. *Nat Rev Cardiol* 17:52-63
205. Zhang W, Deng W, Zhou L, Xu Y, Yang W, et al. 2015. Identification of a juxtamembrane mechanosensitive domain in the platelet mechanosensor glycoprotein Ib-IX complex. *Blood* 125:562-9